The Thesis Committee for Meredith Guenevere Longshore Brown
Certifies that this is the approved version of the following thesis:

Combined effects of global warming and a shutdown of the Atlantic meridional overturning circulation on West African and European climate

APPROVED BY
SUPERVISING COMMITTEE:

Supervisor:

_____
Kerry H. Cook

_____
Rong Fu

_____
Robert E. Dickinson

_____
Charles S. Jackson

Combined effects of global warming and a shutdown of the Atlantic meridional overturning circulation on West African and European climate

by

Meredith Guenevere Longshore Brown, B.S.

Thesis

Presented to the Faculty of the Graduate School of

The University of Texas at Austin

in Partial Fulfillment

of the Requirements

for the Degree of

Master of Science in Geological Sciences

The University of Texas at Austin

May 2012

Acknowledgements

Since I started graduate school in the fall of 2009, my life has changed in many unexpected ways, from changing graduate programs in my first year, to deciding to transition away from academia. I could not have known when I started that this is where I'd end up. Many people helped me a long the way and I'd like to take a minute to thank as many as I can.

First, I'd like to thank my adviser, Dr. Kerry Cook. She took me into her research group after just two meetings. Kerry has been a wonderful adviser, she has always been patient and encouraging of my ideas and the direction I wanted to pursue, even it was unclear where I was headed. There is no other adviser I would rather have had. Second, I'd like to thank my first adviser, Dr. Steven Moore. Although he was only my adviser for one year, he was incredibly supportive of my decision to change programs, without his encouragement to join Kerry's group, I might never have finished graduate school.

Next, I'd like to thank my thesis committee: Dr. Rong Fu, Dr. Robert Dickinson and Dr. Charles Jackson. All three read my thesis drafts quite quickly, despite extensive travel and their many other obligations to their own students, to their research and to their teaching. In particular, Charles Jackson's comments were invaluable to me in editing my thesis.

The Cook research group (Dr. Ned Vizy, Naresh Neupane, Dr. Bing Pu, Dr. Christina Patricola, Dr. Julien Cretat and Jamie Favors) also deserves some special attention for all their help interpreting my findings and refining my thesis. Ned was an indispensable teacher when I first joined the group and has always taken the time to

answer my questions and fix any technical problems that arose. Naresh, Bing and Jamie, you were the best office mates, you always helped keep the mood light and fun.

I'd also like to thank Benjamin Wagman for listening to my presentations and helping me improve them. Next, a special thank you to Stephen Bond, Stephen was always available when I needed a hand, whether it was borrowing his laptop or talking me out of hysteria, I could always count on him for support. And, Nicole Conti, thank you for everything. Thank you for bearing with me through a year and a half of grad school and helping me find my priorites. Thank you for listening to me vent and reassuring me that we're all in this together.

Philip Guerrero also deserves special thanks. Philip is a spectacular graduate coordinator, if ever there was a problem, Philip could usually fix it immediately. Philip is very sympathetic to the emotional toll that graduate school can take; and through his ability to solve problems and general disposition, he has made graduate school that much better for me and so many others.

Finally, and above all, I'd like to thank my parents and my brother for being the best family I could ever ask for. Without your constant encouragement, reminding me of all that I can be, I would not have made it. Thanks guys!

Abstract

Combined effects of global warming and a shutdown of the Atlantic meridional overturning circulation on West African and European climate

Meredith Guenevere Longshore Brown, M.S.Geo.Sci.

The University of Texas at Austin, 2012

Supervisor: Kerry H. Cook

The Atlantic meridional overturning circulation has a vast potential for abrupt climate change due to its large heat transport through the ocean and its nonlinear dynamics. Because of these unique properties, this paper investigates how the climate of West Africa and Europe will respond to a shutdown of the Atlantic meridional overturning circulation at the end of the 21st century. Here we use a regional climate model with 90-km grid spacing is forced by an idealized sea-surface temperature anomaly, based upon coupled atmosphere/ocean global model water hosing experiments, with a business-as-usual global warming scenario to discover how West African and European climate will change.

In both the boreal spring and summer, cooling in the eastern Atlantic is associated with a strong intensification and eastward extension of the North Atlantic subtropical high over Europe throughout the depth of the atmosphere, a strengthening of the heat low

over West Africa at low levels, and a weakening of the Saharan High in the upper atmosphere. Rainfall rates also decrease markedly throughout most of West Africa and Europe: in spring, rainfall rates decrease by 50-80% over Sahelian Africa, in summer rainfall over Europe decreases by up to 90%, while precipitation over West Africa is reduced by 40%.

Table of Contents

List of Figures

Chapter 1: Introduction

The importance of studying the abrupt climate change potential of the Atlantic meridional overturning circulation (AMOC) comes from two unique properties: the AMOC transports substantial heat poleward, and it exhibits nonlinear dynamical behavior (Stouffer 2006). It is believed that large inputs of freshwater into the North Atlantic, such as glacier and polar ice melt due to global warming, could trigger a weakening or total collapse of the AMOC (Manabe and Stouffer 1988, 1995; Schiller et al. 1997; Wood et al. 1999; Vellinga and Wood 2002; Clark et al. 2002; Rahmstorf 2002), however, there is considerable uncertainty as to the likelihood of an AMOC shutdown because different coupled atmosphere-ocean GCMs (AOGCMs) disagree on the time it takes for the AMOC to respond to freshening of the North Atlantic, or even if the AMOC responds at all. AOGCMs that do simulate a weakening or shutdown of the AMOC disagree on the magnitude of weakening, and AOGCMs disagree on the time it would take the AMOC to recover to its current state after the forcing has been applied (e.g. Thorpe et al. 2001; Vellinga and Wood 2002, 2008; Hu et al. 2004; Gregory et al. 2005; Schmittner et al. 2005; Ridley et al. 2005; Jungclaus et al. 2006; Stouffer et al. 2006; Swingedouw et al. 2007; Meehl et al. 2007).

Despite the uncertainty of an AMOC shutdown, the climate consequences which are varied and uncertain are potentially severe (e.g., Ganopolski et al. 1998; Kuhlbrodt et al. 2009). The tropical ocean temperature could rise, due to decreased heat transport, and affect the atmosphere's temperatures and Atlantic ocean salinity would change as the temperature changed (e.g., Vellinga and Wood 2002, 2008; Chang et al. 2008; Laurian et

al. 2009b, Lenton 2008). Atlantic ocean temperatures have been linked to rainfall rates in the West African Sahel region, a region which receives the majority of its rainfall during the monsoon season, and therefore changes in rainfall duration or intensity could pose a significant problem for people in that area (Chang et al. 2008). With increased ice melt in the north Atlantic, sea levels could rise, endangering coastal communities and economies (Kulhbrodt 2009). The climate consequences for global warming, including increased ice melt which could trigger a shutdown of the AMOC, are also of great concern to people living in West Africa and Europe (Vizy and Cook 2006, Patricola and Cook 2010).

There are many studies which have used AOGCMs to predict the climate effects of global warming on the strength of the AMOC and on the earth's climate (Stouffer et al. 2006, Vellinga and Wood 2002, 2008), and there are regional studies investigating the effects of global warming, particularly on the climate of West Africa (Vizy and Cook 2006, Patricola and Cook 2010), however there are no regional or seasonal studies in the literature up to this point which combine the two potentially high impact events on West African and European climate.

In order to fill this hole in the literature, this paper seeks to answer the question: How do global warming and a shutdown of the AMOC affect the climate of West Africa and Europe and the end of the 21st century? To answer that question, a regional climate model is used to optimize the simulation of late-20th c. climate over West Africa and Europe at as fine a spatial resolution as the most advanced GCMs (Vizy and Cook 2006; Patricola and Cook 2010). For the end of 21st c. simulation, and idealized sea-surface temperature (SST) anomaly is imposed on the 20th c. SSTs and a business-as-usual CO_2 scenario is selected. This paper focuses on West Africa and Europe during the warm

season (May-September), the seasons, spring (May-June) and summer (July-September), are chosen based on the African rainy period because of the importance of African monsoon.

The study is presented in the following order: the motivating literature review is in section 2, in section 3, a description of the model and the analysis tools used, section 4 shows the validation of the model results to the present-day observed climatological features. Results are presented in section 5 and conclusions will be given in section 6.

Chapter 2: Background

Recent ocean and climate studies (e.g., Wood et al. 1999; Thorpe et al. 2001; Clark et al. 2002; Rahmstorf 2002; Schmittner 2005) suggest that anthropogenic global warming will result in a weakening of the AMOC by the end of this century, but there is a disagreement among models as to the degree of the weakening (e.g., Fichefet et al. 2003; Swingedouw et al. 2006, 2007, Latif et al. 2000; Ridley et al. 2005; Jungclaus et al. 2006; Gerdes et al. 2006; Vizcaino et al. 2008).According to the Intergovernmental Panel on Climate Change Fourth Assessment Report (IPCC AR4), it is less than 10% likely that a complete shutdown will occur by 2100 (Meehl et al. 2007).

The disagreement among models as to the weakening of the AMOC arises from unknown mechanisms which support the stability of the AMOC. Manabe and Stouffer (1988, 1995) found that the AMOC has two stable equilibria, active and inactive, but the mechanisms by which the AMOC transitions from one state to the other are not well known. Since the AMOC is part of the global thermohaline circulation, changes in the AMOC should be caused by temperature and salinity changes in the mixed-layer, particularly in the North Atlantic where formation of deep water occurs (Lenton et al. 2008). However, not all the models which aim to force an AMOC shutdown by freshening the North Atlantic simulate a collapse of the AMOC. Some studies show substantial weakening or stopping of the AMOC (e.g., Fichefet et al. 2003; Swingedouw et al. 2006, 2007), while others show negligible changes to the AMOC, or that the ocean circulation recovers soon after the initial forcing is ceased (e.g., Latif et al. 2000; Ridley et al. 2005; Jungclaus et al. 2006; Gerdes et al. 2006; Vizcaino et al. 2008).

Most studies that simulate a weakening or collapse of the AMOC find that surface temperatures in the North Atlantic cool due to the influx of cold, freshwater. South of the equator, temperatures increase because the AMOC is not working to transport heat northward (e.g., Vellinga and Wood 2002, 2008; Chang et al. 2008; Laurian et al. 2009b; Wen et al. 2010; Laurian and Drijfhout 2011). There is a large range in modeled sea-surface temperature (SST) changes due to changes in the AMOC, for example Swingedouw et al. (2006) found that a weakened AMOC decreased globally averaged SSTs by 0.44 K after 70 years, while Laurian et al. (2009b) found a global surface cooling of 0.72 K.

The atmospheric climate effects resulting from inducing a weakening or shutdown of the AMOC are also varied (Kuhlbrodt et al. 2009). For the climate over Africa, Chang et al. (2008) found that cooler SSTs in the North Atlantic increase the land-sea temperature gradient which, according to previous studies of the African monsoon variability (e.g., Lamb 1978; Folland et al. 1986; Fontaine and Janicot 1993; Vizy and Cook 2001), should affect monsoon flow and surface evaporation and have large implications for precipitation. Over Europe, Brayshaw et al. (2009) found that during the winter the North Atlantic storm track penetrated further into Western Europe while Laurian et al. (2009a) found decreased precipitation. Several studies also found a southward shift of the ITCZ (e.g., Zhang and Delworth 2005; Stouffer 2006), which led to decreased precipitation in the tropical Atlantic north of the equator (e.g., Vellinga and Wood 2002, 2008; Jacob et al. 2005; Zhang and Delworth 2005; Stouffer 2006; Chang et al. 2008, Wen et al. 2010).

According to the literature, it is unlikely that the AMOC will shutdown by the end of the 21st century, however there is no consensus as to the climate effects of such an event. Therefore, this paper takes a worst case scenario position and asks how the climate of West Africa and Europe will respond to a shutdown of the AMOC and global warming.

Chapter 3: Methodology

EXPERIMENTAL DESIGN

The regional model used to conduct a late-20th c. control simulation and a late-21st c. future simulation is the National Center for Atmospheric Research/ National Oceanic and Atmospheric Administration (NCAR/NOAA) Weather Research and Forecasting model (WRF; Skamarock et al. 2005) version 3.1.1. The model uses 30 vertical σ-levels, with the top of the atmosphere set at 30 hPa, 90-km horizontal grid spacing, and a model time step of 4 minutes. This horizontal resolution is selected based on previous regional modeling results (e.g., Patricola and Cook 2010; Neupane and Cook 2011; Vizy and Cook 2011) which demonstrate that WRF can realistically simulate the boreal summer climate over Africa, the North Atlantic, and North America at this resolution. This resolution, while comparable to the most state-of-the-art AOGCMs, is finer than previous models [i.e., Coupled Model Intercomparison Project (CMIP3) IPCC AR4 AOGMs] and can provide detailed spatial information. Also, by using a regional model, physical parameterization selection can be optimized for simulating rainfall over West Africa and Europe in order to produce a realistic simulation of the regional climate state.

Figure 1 shows the model domain. A domain which encompasses the entire Atlantic between 5°S to 70°N as well as most of the continental United States, Western Europe, and northern Africa is chosen to study the effect of changes in the AMOC on the regional climates of the adjacent land masses. The focus of this paper is on northern

7

Africa and Europe, while a companion paper, Pu et al. (2011), focuses on the impacts of an AMOC shutdown over North America.

The physical parameterization selections are the same as Patricola and Cook (2010), except that the RUC land surface model (Smirnova et al. 1997, 2000) is replaced by the unified Noah land surface model (Chen and Dudhia 2001), as it was found to yield more realistic results over the entire domain. Physical parameterizations used include the Mellor-Yamada-Janjic planetary boundary layer scheme (Mellor and Yamada 1982; Janjic 1990, 1996, 2002), the Monin-Obukhov-Janjic surface layer scheme (Monin and Obukhov 1954; Janjic 1994, 1996, 2002), the new Kain-Fritsch cumulus convection scheme (Kain and Fritsch 1990, 1993) , the Purdue Lin microphysics scheme (Lin et al. 1983; Rutledge and Hobb 1984; Tao et al. 1989; Chen and Sun 2002), the RRTM longwave radiation scheme (Mlawer et al. 1997), and the Dudhia shortwave radiation scheme (Dudhia 1989). SSTs are prescribed and updated every 6 hours.

Two ensemble experiments are conducted a late-20th c. control experiment and a late-21st c. future AMOC shutdown and global warming experiment. Each ensemble consists of 20 integrations, enough to be averaged together to form a climatology. Each integration is initialized on March 15th and run for 200 days, terminating after September 30th. The first 17 days of every integration are devoted to model spin-up and not used for analysis.

The first ensemble is a late-20th c. control (Control) experiment. These integrations use the National Center for Environmental Prediction reanalysis 2 (NCEP2; Kanimitsu et al. 2002) interpolated onto the regional mode grid to specify initial and lateral boundary conditions. 6-hourly values of winds, temperature, relative humidity,

surface temperature, mean sea-level pressure, SST, soil temperature, and soil moisture are utilized to formulate the necessary boundary conditions. Soil moisture and soil temperature are initialized on 15 March of each year and then updated by the land surface model. Conditions from individual years from 1981 through 2000 produce the needed boundary conditions for each of the 20 integrations of the ensemble. Thus, initial and lateral boundary conditions preserve the 6 hourly transient activity of the individual years, producing variations among the 20 members of the ensemble. The CO_2 concentration is held fixed at 330 ppmv.

The second ensemble is a projected late-21st c. AMOC shutdown which uses a CO_2 concentration of 757 ppmv, the 2081-2100 average CO_2 concentration of the IPCC AR4 A2 "business as usual" emissions scenario (Shutdown) experiment. Effects of other greenhouse gases and aerosols are not included in the regional model. Based on the IPCC AR4, the A2 emissions scenario represents an upper limit of the expected change in CO_2 concentration. For this simulation, the source of the shutdown in the AMOC is an influx of high latitude meltwater of sea ice and ice sheets which we simulate by prescribing the SSTA pattern from ocean models (e.g., Vellinga and Wood 2002, 2008; Stouffer et al. 2006; Barreiro et al. 2008; Chang et al. 2008). Results from the coupled AOGCMs that are part of the IPCC AR4 do not indicate a shutdown of the AMOC by the end of the 21st c., only a slowdown with an average reduction of 25% ± 25%, depending on the model (Meehl et al. 2007).

The initial and lateral boundary conditions for the future shutdown ensemble are generated by adding anomalies from the IPCC AR4 AOGCM A2 scenario and applying these anomalies to the NCEP2 reanalysis late 20th c. control conditions. This differs from

9

a conventional downscaling approach where GCMs would be used to generate both the late 20th c. control and 21st c. future conditions by using GCM full fields directly. This study does not use this downscaling approach because it is important to have an accurate control simulation, and using initial and lateral boundary conditions derived directly from the AOGCMs has been shown to degrade the results in other regional climate model applications (e.g., Seth and Rojas 2003; Rojas and Seth 2003; Cook and Vizy 2008; Patricola and Cook 2010).

For this study an AOGCM anomaly for each field is produced by differencing the climate of the 20th c. experiment 1981-2000 climatological monthly mean value averaged over 9 models (i.e., CGCM3.1 (T47), CNRM-CM3, ECHAM/MPI-OM, GFDL-CM2.0, MIROC3.2 (medium resolution), MRI CGCM2.3.2, NCAR CCSM3, NCAR PCM, and the UKMO-HadCM3) from the 2081-2100 A2 emissions scenario climatological monthly mean value averaged over the same 9 AOGCMs. These multi-model climatological monthly mean anomalies are then assumed to be the mid-month values and linearly interpolated to produce anomalies every 6 hours. The 9 AOGCMs are selected to provide a range of uncertainty across the models, and are the same 9 models used by Patricola and Cook (2010). Note the approach used here differs from Patricola and Cook (2010) in that instead of running ensembles with variability of each member forced by the individual AOGCM anomalies, here ensemble members vary based on the transient activity from the present day NCEP2 reanalysis. The transient activity from each of the 20 late 20th c. control integrations is being preserved, but it is applied to a different climate state associated with global warming under the A2 scenario from the AOGCM multi-model mean.

The IPCC AR4 AOGCMs do not provide output to determine future soil moisture and soil temperature anomalies. Given the lack of a better option, the present day initializations for each of the 20 years for the future AMOC shutdown ensemble are used. This decision seems justified since the examination of the soil moisture and soil temperature fields over Africa from test integrations reveal that they adjust to the overlying atmospheric conditions, usually within a couple of weeks (i.e., within the spin-up period).

An idealized AMOC shutdown SSTA pattern is designed and applied to the control SSTs for each integration using results from published water-hosing experiments (e.g., Vellinga and Wood 2002, 2008; Stouffer et al. 2006; Barreiro et al. 2008; Chang et al. 2008) as a reference, then adding anomalies to represent greenhouse gas-induced warming. These AOGCM water-hosing studies indicate the development of a North Atlantic cooling minimum centered south of Greenland with magnitudes ranging between -5 to -12 K. Since the SSTAs from the water hosing experiments are annual mean anomalies and this study is focused on the boreal summer months, a more modest – 7 K minimum magnitude centered at 20ºN and 55ºW is selected and a Gaussian shaped cooling center in the North Atlantic is applied. SSTs in the eastern boundary current (e.g., the Canary Current) are also simulated to cool in these water hosing experiments, but to a lesser extent, so a comma-like cold anomaly pattern is designed where SSTAs gradually warm as they approach the equator. While there is some modeling evidence (e.g., Chang et al. 2008; Stouffer 2006; Vellinga and Wood 2008) that suggests that the tropical Atlantic/South Atlantic may warm due to an AMOC shutdown, the degree of warming is uncertain and may well be delayed. No warming due to the shutdown of the

AMOC was applied in the tropical Atlantic for these integrations, so the results presented here are dependent upon this caveat.

Finally, to place this idealized SSTA pattern in the framework of global greenhouse gas warming, a +2.5 K SSTA is applied to every water point in the domain. 2.5 K is the domain averaged SSTA calculated for the 2081-2100 AOGCM multi-model ensemble mean for the IPCC AR4 A2 emissions scenario. Over the Mediterranean the +2.5K anomaly is offset by the projected AMOC shutdown signal (Stouffer et al., 2006), so the net SSTA change in the Mediterranean is small. Figure 1 shows the idealized SSTA applied for the future shutdown simulations.

ANALYSIS TOOLS

To relate the rainfall to the large-scale circulation, the vertically-integrated, mass-weighted moisture budget (discussed in detail in Lenters and Cook 1995) is calculated for the 20th century control and future shutdown climatologies. In this approach the climatological precipitation rate, $\overline{P}$ is equal to the evaporation rate, $\overline{E}$ minus the vertically integrated water vapor flux divergence and the local time rate of change of the mixing ratio:

$$\overline{P} = \overline{E} - \overline{\int_0^1 p_s \left[\vec{\nabla}_{3P} \cdot q\vec{u}_{3P} + \left(\frac{\partial q}{\partial t} \right)_p \right] \frac{d\sigma}{g\rho_w}} \tag{1}$$

Where p_s is the surface pressure, $\vec{\nabla}_{3P}$ is the three-dimensional divergence operator in pressure coordinates, $\vec{u}_{3P}$ is the three-dimensional wind velocity vector, g is the acceleration due to gravity, ρ_w is the density of water and $d\sigma$ is the sigma-level

thickness. Because this is a time mean, the third term on the RHS of the Eq. 1 is neglected.

Eq. 1 can be further decomposed into its time-mean and transient components; the divergence operator can be expanded into vertical and horizontal components; the vertical derivative evaluated; and the integral rewritten as a finite sum to produce:

$$P = C + A + O + T + E \tag{2}$$

Where all of the variables in equation 2 are climatological means, and

$$C = -\frac{p_s}{g\rho_w} \sum_{\sigma=0}^{1} \left(q\vec{\nabla}_{2p} \cdot \vec{u}_2 \right) \Delta\sigma \tag{3}$$

$$A = -\frac{p_s}{g\rho_w} \sum_{\sigma=0}^{1} \left(\vec{u}_2 \cdot \vec{\nabla}_{2p} q \right) \Delta\sigma \tag{4}$$

$$O = -\frac{1}{g\rho_w} \left(q\omega \right)_s \tag{5}$$

$$T \approx -\frac{1}{g\rho_w} \vec{\nabla}_2 \cdot \left[\int_0^1 \left(\overline{p_s q\vec{u}_2} - \overline{p_s} \, \overline{q\vec{u}_2} \right) d\sigma \right] \tag{6}$$

Eq 3, the moisture convergence term, represents the precipitation associated with horizontal wind convergence, Eq 4, the moisture advection term, is the precipitation associated with horizontal moisture advection. Eq 5 is the orographic term, or the precipitation associated with the presence of topography, which is estimated here as part of the residual, defined as:

$$O = P - (E + C + A + T) \tag{7}$$

13

Therefore, O includes orographic precipitation plus numerical error from the calculations. Finally Eq 6 is the transient eddy term, discussed in greater detail in Lenters and Cook (1995).

Chapter 4: Validation

To validate the control experiment, a comparison is made of the model's precipitation, geopotential height and wind climatology to observational and reanalysis climatology. For precipitation, it is most important for the model to capture the spatial distribution of rainfall. One of the advantages of an RCM over a GCM is that the model's parameterization schemes can be optimized or "tuned," as was done in this experiment, to capture an accurate rainfall distribution as observed by satellite or ground station. For the geopotential height and wind fields, a good simulation will capture the position of notable atmospheric features, such as the North Atlantic subtropical high (NASH) and the continental heat low at low levels, and the Saharan high at high levels. Other features, such as the West African westerly jet and the African easterly jet are also prominent features, but most important to this study are the NASH, the continental heat low and the Saharan high.

PRECIPITATION

The precipitation validation is shown in Figure 2. The model has a wet bias in all seasons, but the seasonal cycle of rainfall and the spatial distribution are well simulated. Figure 2a shows the 1979-2006 precipitation climatology recorded by the Climate Research Unit (CRU; Mitchell and Jones 2005) TS3.0 over the land surface and the NASA Global Precipitation Climatology Project (GPCP) V2.1 (Adler et al. 2003) over the ocean averaged for May and June (MJ) for the African spring. The CRU TS 3.0 climatology has a spatial resolution of 0.5°, but it is only available over land, while the GPCP product has a coarser resolution (2.5°), but covers both the land and ocean; by

15

blending the CRU and the GPCP climatologies, a single dataset is obtained, with high spatial resolution over land, which can be used to validate the present-day control simulation.

Over the tropics a main precipitation band associated within the ITCZ is positioned between the equator and 10°N, with the highest intensity rainfall (up to 10 mm/day) located near the coasts of Sierra Leone and Liberia (7°N, 11°W). Between 15°N and 30°N over Africa rainfall is sporadic with generally less than a trace (0.25 mm/day). Over Europe, the largest MJ rainfall rates up to 8 mm/day are located over the Alps from 44°N to 48°N and 5°E to 15°E. Elsewhere over Europe, precipitation rates generally range between 2 and 4 mm/day.

Figure 2b shows the MJ precipitation climatology from the late 20th c. control ensemble. The regional model simulates the MJ precipitation distribution well, but over Africa, south of 10°N, between 20°W and 30°E, rainfall rates are larger than observed by 4-10 mm/day, 40-60% more rainfall than observed. Over Europe, precipitation rates are generally overestimated by 2 mm/day. There is also a domain edge effect along eastern boundary east of 20°E. The analysis is focused west of 20°E to exclude this edge effect.

Figures 2c and 2d show the July, August and September (JAS) precipitation climatologies; CRU/GPCP estimates and late 20th c. control, respectively. The observations (Fig. 2c) indicate that the rainband over the tropics shifts northward , from the Guinean coast (5°N), to approximately 8°N over West Africa, while rainfall increases over the Sahel (12-17°N).), while rainfall intensity also increases over West Africa as precipitation rates are 2-4 mm/day higher during the summer than in the late spring. Over continental Europe the rainfall intensity is generally lower (i.e., by ~ 2 mm/day) in

the summer compared to the late spring. Three local maxima are observed, one over the Alps (44°N-48°N, 5°E-15°E), one over Scotland (55°N, 9°W), and one along the coast of Norway at about 60°N and 5°E.

Similar to MJ, during JAS the regional model simulates the distribution of the observed precipitation (Fig. 2d) reasonably well, but has a wet bias. The model overestimates precipitation rates by 4 mm/day or more between 5°N and 15°N over West Africa. Between 35°N and 52°N the modeled precipitation rates are about 2 mm/day more than observed, while the model underestimates the Norway maximum (60°N, 5°E). Overall, the model has a wet bias in the tropics, but it does capture the regional spatial distributions of the precipitation signal as well as its seasonal evolution.

CIRCULATION

The following describes the circulation validation, shown in Figures 3 and 4. The most important features for this study are the NASH and the continental heat low at low levels and the Saharan high in the upper levels. In both spring and summer of the control experiment, the NASH is stronger and extends further up into the atmosphere, the continental heat low is lower and encroaches on the west coast of West Africa, and the Saharah high is more intense the reanalysis.

May-June

Fig. 3a shows MJ 850-hPa geopotential heights and winds from the NCEP2 climatology. The North Atlantic subtropical high (NASH) is centered at approximately 28°N and 49°W. The height gradient is relatively strong on the northern flank of the NASH between 40°N and 55°N compared to the gradients to the east and south of the

NASH. Associated with the NASH's anticyclonic flow are westerly winds across Europe which turn northerly across the Mediterranean and North Africa, with some easterly flow at 20°N from 10°E to 20°E; and easterly winds coming off West Africa south of 20°N. Another important feature of the 850 hPa geopotential height field is the heat low over West Africa. In the reanalysis the heat low covers most of West Africa at 900 hPa (not shown), however at 850 hPa the it is still evident.

Fig. 3b shows the MJ control 850 hPa geopotential heights and winds. The regional model places the NASH approximately 3° latitude north and 11° longitude east of the NCEP2 reanalysis climatological location and it is up to 20 geopotential height meters stronger at the center, while the high pressure over Libya (i.e., 25°N-35°N, 0°E-20°E in the reanalysis) is smaller in extent and shifted eastward 10° longitude and southward 3° latitude. Examination of the MJ 850 hPa geopotential height climatology from the ERA Interim reanalysis (not shown) indicates a further east positioning of the NASH (i.e., centered at ~ 29°N and 42°W) compared to the NCEP2 with approximately the same strength. The flow on the northern flank of the modeled NASH is in the same direction and magnitude as the reanalysis, while the monsoon trough over Africa is deeper in the model denoted by the lower geopotential heights and stronger winds over West Africa between 5°N and 20°N. Also, 850 hPa winds from the Gulf of Guinea is more southerly in the control and appear to turn westerly between 5°N and 10°N. The heat low over continental West Africa in the model extends all the way to west coast, and north into the Sahara up to 20°N. The validation figures are for 850 hPa, rather than 900 hPa, because while the features of interest are well simulated spatially through the depth

18

of the atmosphere, at 900 hPa (not shown) the model calculates geopotential heights 300-350 gpm higher than the reanalysis at that level.

In Figure 3c the 600 hPa NCEP2 MJ geopotential height (gpm) and wind (m/s) climatology shows the Saharan high centered at 20°N, 0°E. The flow at 600 hPa is westerly north of 20°N and turns easterly around the Saharan high south of 20°N.

Figure 3d is the 600 hPa control simulation MJ geopotential height (gpm) and wind (m/s) climatology. In the model, the Saharan high is also centered at 20°N, 0°E, but it extends further east and west to 20°E and 30°W respectively. Over the ocean there is also a ridge of high pressure at ~48°N, from 50°W to 30°W which is not in the reanalysis. This ridge, which resembles the northern flank of the NASH, extends upwards in the atmosphere to 150 hPa (not shown).

July-September

Fig. 4a shows the observed 850 hPa geopotential heights for JAS from the NCEP2 reanalysis. In JAS, the model (Fig. 4b) simulates the same intensity and location of the NASH, but the heat low over Africa is lower in the model than in the NCEP2 reanalysis. The modeled low geopotential heights centered at 10°N, 20°E are associated with a stronger gradient between the land and the ocean than in the reanalysis, which in turn is related to stronger low-level westerly (easterly) flow between 5°N and 10°N (15°N and 25°N). Also, in subtropical Africa (0°-15°N) the 850 hPa winds are south-easterly from 50°W to 10°W.

At 600 hPa, the NCEP2 reanalysis (Fig. 4c) shows the Saharan high centered at 25°N, 5°W, and just as in MJ, the flow is westerly north of the high and turns easterly

south of the high. In the model (Fig. 4d) the Saharan high is stronger than in the reanalysis, but centered in the same location. As in MJ, there is ridge of higher pressure over the ocean, consistent with the intensified NASH throughout the depth of the atmosphere.

The validation analysis indicates that the regional model can realistically simulate the late boreal spring and summer climate over northern Africa and Europe. While there are some differences between the observations and the model results, the spatial and seasonal distribution of precipitation is accurate and all of the important circulation features are captured, the NASH, the continental heat low, and the Saharan high. Furthermore, the overestimated precipitation and the intensified geopotential height and stronger winds are internally consistent with each other, suggesting that the discrepancies between the model and the observations are due to the model's precipitation parameterization scheme.

Chapter 5: Results

To determine how the climate of West Africa and Europe respond to the increased CO_2 due to global warming and the AMOC shutdown SSTA, the anomalous precipitation and circulation fields are examined. Linking precipitation and wind, is the vertically-integrated, mass-weighted moisture budget. In this section, the moisture budget will be presented followed by the changes to circulation for each season.

Most important to this study is to see how precipitation on the coast of West Africa and over Europe is supported by the terms in the moisture budget in the control experiment, and compare that to how precipitation changes are supported in the anomaly fields. In particular, over West Africa, moisture convergence (Eq. 3) and moisture advection (Eq. 4) will be important, and over Europe, evaporation, transient eddies (Eq. 6) and orographic precipitation (Eq. 5) will predominantly support precipitation. From the moisture budget calculations, precipitation can be linked to circulation, and while causality may not be determinable, the changes to the circulation features consistent with the changes to precipitation can be linked to the SST forcing and increased atmospheric CO_2.

MAY-JUNE

Moisture Budget

The six terms of atmospheric moisture budget (Eq 2) for the control climatology, averaged over May and June (MJ) are shown in figure 5. The moisture budget includes the precipitation (Fig. 5a), evaporation (Fig.5b), moisture convergence (Fig. 5c), moisture

advection (Fig. 5d), moisture transients (Fig. 5e), and orographic (Fig. 5f) terms. Each panel is shaded to the same scale as precipitation field.

The precipitation climatology is shown in Figure 5a, the same as Figure 2a, but with a different shading scale. Fig. 5b is the evaporation term. Over land, the spatial structure of the evaporation field is generally similar to that of the precipitation (Fig. 5a), but evaporation rates are smaller than precipitation rates in West Africa (i.e., $2-6$ mm/day compared to greater than 8 mm/day for precipitation), except over the Sahara where both are negligible. Over West Africa (i.e., 5°N-15°N, 15°W-10°E) evaporation supplies approximately 48 % of the available moisture. Over Europe the evaporation rates are generally equal to, and in some places greater than that of the precipitation rates. Over western Europe (38°N-55°N,10W-15°E) evaporation accounts for 108% of the water available for precipitation.

The moisture convergence term (Eq. 3) is shown in Figure 5c. Over West Africa this term contributes positively toward rainfall and accounts for ~95% the precipitation along the Guinean coast (i.e., 4°N-6°N, 10°W-10°E). 85% of the moisture convergence signal is associated with meridional moisture convergence, related to the strong low-level moisture influx from the Gulf of Guinea. Over Europe, and West Africa north of 20°N, the convergence term and the moisture advection term (Eq. 4, Fig. 5d) have very similar spatial structures, and opposite signs of nearly the same magnitude. To first order, horizontal moisture convergence and horizontal moisture advection balance each other out, meaning that the divergence of the horizontal moisture flux is zero. Thus, over Europe, the net contribution of moisture convergence and moisture advection is

negligible. The advection term is small over West Africa, and contributes less than 1% towards precipitation.

The transient eddy term (Eq. 6) is given in Figure 5e. Averaged over the whole analysis domain (shown) the transient eddy term is nearly zero. North of 20°N however, they do contribute positively towards precipitation in areas with topography. And in West Africa, positive transient eddies occur north of 10°N with negative transient eddies south of 10°N mainly from the meridional transient eddy term. The residual term (Eq.7, Fig. 5f) is nearly zero over the majority of the analysis domain; however, over Europe, the Atlas Mountains and the Cameroon highlands, the residual term resembles the pattern of topography.

As expected, over West Africa meridional moisture convergence is the largest contributor to precipitation due to the southerly flow from the Gulf of Guinea, while over Europe, precipitation is supported by evaporation, transient eddies and the residual term which includes orographic precipitation.

Figure 6 shows the future AMOC shutdown anomaly fields for the moisture budget terms for May/June. Africa and Europe are both projected to be drier (Fig. 6a).Over West Africa (5°N-15°N, 10°W-20°E) rainfall rates decrease by up to 6 mm/day, a 20-40% reduction in rainfall. Across southern Europe (37°N-42°N) 1-2 mm/day decreases in rainfall are equivalent to a reduction in rainfall of up to 80%, while over northern Europe (42°N-65°N), 1-3 mm/day decreases correspond to a 20-40% reduction.

The evaporation anomaly (Fig. 6b) shows decreased evaporation in the north Atlantic ocean where cool SSTAs were applied, and increased evaporation over the tropical and subtropical ocean where warm SSTAs were applied, except in the Gulf of

Guinea where there is an area just off the southern coast of increased evaporation with decreases in evaporation elsewhere. Over the Mediterranean Sea the anomaly is nearly zero mm/day, which physically corresponds to the fact that no change in SST was applied to the Mediterranean. There is increased evaporation along the Guinean Coast 4°N-6°N,10°W-10°E), Central Africa below 6°N, over the Alps (42°N-47°N, 0°E-15°E), in northern Spain (43°N, 10°W-0°E), and in the Scandinavian countries north of 57°N, between 10°E and 20°E. Again, areas east of 20°E, while shown in the figures, are not analyzed because of the large edge effect.

The convergence anomaly (Fig. 6c) has a very similar structure to and represents 147% of the precipitation anomaly averaged from 0°N-11°N, 50°W-20°E, with areas of positive anomalous convergence over areas of topography. The excess drying in the moisture convergence term between 0°N and 11°N is accounted for in the evaporation term (Fig. 6b) and the three remaining moisture budget terms. There is a strong dipole in the anomalous convergence signal in central Europe, around the Alps (42°N-48N, 5°E-15°E), which is well matched in structure by the moisture advection anomaly (Fig. 6d), but is of opposite sign and   ~60% of the magnitude. When added together, the convergence and advection term, or the convergence of the moisture flux, contribute to drying over most of Europe with the same dipole pattern as the convergence term around European topography. Thus, the moisture flux convergence contributes to anomalous drying on the windward side of topography and anomalous increases in precipitation on the leeward side, which are negated by the transient and residual terms, Fig.6e and 6f respectively.

The transient eddy anomalies (Fig. 6e) are negligible over most of West Africa, with a band of positive anomalies from 10°N to 17°N and 8°W to 25°E. These positive anomalies occur mainly in the meridional transient term and are most likely associated with increased north-easterly flow around the extended high over Libya (shown in Figure 7). Negative anomalies in the moisture advection term (Fig. 6d) between 10°N and 17°N cancel with the positive transient anomalies over West Africa. Over Europe there are positive transient (Fig. 6e) and residual (Fig. 6f) anomalies over the Mediterranean, southern Spain and from the Alps northward. Together with the advection term (Fig. 6d), the transient and residual anomalies form a dipole of positive contributions towards rainfall north of the Alps and negative contributions towards rainfall south of the Alps, which compensate for the positive anomalies in the convergence anomaly (Fig. 6c).

In summary, over West Africa, moisture convergence (Fig. 5c) and moisture advection (Fig. 5d) support precipitation (Fig. 5a), and the moisture convergence anomaly (Fig. 6c) accounts for the 20-40% reduction in rainfall (Fig. 6a). While over Europe, evaporation (Fig. 5b), transient eddies (Fig. 5e) and the residual term (Fig. 5f) account for precipitation (Fig. 5a), and all the terms (Fig. 6b-f) support the anomalous reductions in rainfall.

Circulation

Figure 7a shows the 850 hPa MJ future shutdown climatology geopotential height (gpm) and wind (m/s), while Figure 7b shows the future shutdown minus the 20th century control simulation differences. Fig. 7c is the 600 hPa MJ future geopotential height (gpm) and wind (m/s) climatology, and Fig. 7d is the 600 hPa geopotential height and wind

anomaly for MJ. Note the geopotential height anomalies have been normalized by subtracting the domain averaged May/June increase in geopotential height (i.e., 25 gpm) to better highlight the changes in the geopotential gradients. The MJ 850 hPa NASH is centered at 47°N and 5°W, which is approximately the same location as in the control (Fig. 3b). However the NASH extends further eastward and northward across Europe and is associated with stronger westerly low-level flow over the North Atlantic between 20°W and 20°E, from 42°N to 58°N. Over northern Africa the anticyclone south of the Mediterranean Sea has intensified and shifted approximately 10° of longitude to the west. The stronger anticyclone is associated with enhanced northerly flow over eastern Europe, the Mediterranean, and north central Africa, and increased easterly flow over the southern Sahara and Sahel (i.e., between12°N and 25°N). The increase in dry air advection and reduced moisture convergence over the Sahel during the future AMOC shutdown is associated with the stronger anticyclonic flow. Along the Guinean coast, the decrease in moisture convergence is associated with a weakening of the low-level southerly flow. This change is likely associated with the change in the meridional SST gradient, as in the future AMOC shutdown North Atlantic SSTAs cool at mid- to high latitudes, while the tropical Atlantic SSTAs warm creating a larger tropical to high-latitude temperature difference.

Over Europe enhanced anticyclonic flow is associated with decreased wind speeds over Spain (36°N-42N, 8°W-0°E), and with the decreased evaporation in that area (Fig. 6b) accounts for the decrease in precipitation (Fig. 6a). Over Europe from 40°N to 51°N and 0°E to 20°E the anomalous anticyclonic winds lead to decreases in meridional moisture convergence (Fig 6c) and moisture advection (Fig 6d) of up to 6 mm/day, which

is offset by increases in zonal moisture advection (Fig. 6d), increased evaporation over the Alps (Fig. 6b) and increased residual precipitation (Fig. 6f) to yield and overall decrease in precipitation of 2-3 mm/day (Fig. 5a).

At 600 hPa (Fig. 7c) the Saharah high is higher in the shutdown than in the control (Fig, 3d), and the ridge of high pressure over the ocean is relatively weaker compared to the control. The 600 hPa anomaly field (Fig. 7d) shows an increase in geopotential height over Europe and decreases over the ocean and West Africa, similarly to the 850 hPa anomaly (Fig 7b). The anomaly at both levels is consistent with an increase in the NASH, while the heat low and the Saharan high are weakened relative to the increase in the NASH. The MJ anomaly fields, with the NASH increased over land compared to the ocean, are reminiscent of the wintertime NASH (Davis et al. 1997), where the NASH strengthens over the land relative to the ocean due to increased cooling over land compared to the ocean in the boreal winter. This suggests that the imposed SSTA gradient in the North Atlantic is likely the stronger forcing mechanism in changing the position and intensity of the NASH.

JULY-SEPTEMBER

As in the MJ section, the JAS section will detail the moisture budget, paying careful attention to the terms in the moisture budget which support precipitation and the changes to precipitation, followed by the changes to the circulation field. While the details are very similar to the spring time, the summer monsoon brings rainfall into the Sahel, and the NASH moves from its spring time mode to its summertime mode, which is tremendously important for impacts analysis.

27

Moisture Budget

The six terms of Eq. 1 for the JAS control simulation are shown in Figure 8, with each panel shaded to show that terms contribution towards precipitation and stippling over negative values, similarly to Fig. 5.

The JAS future precipitation signal (Fig. 8a) shows that the rainband has moved northward between 6°N and 11°N, bringing rainfall into the West African Sahel (12°N-17°N) and that the European rainfall maximum is located over the Alps at 43°N between 5°E and 15°E, with a secondary maxima over the Scandinavian countries at 8°E, between 57°N and 62°N, the same as Fig. 2d. The evaporation signal (Fig. 8b) shows maximum evaporation over the Mediterranean and the tropical Atlantic Ocean from 2°N-6°N and 30°W-10°W. Over West Africa the structure of the evaporation signal is similar to the structure of the precipitation signal (Fig. 8a), but only accounts for 40% of the precipitation from 15°W-10°E and 5°N -15°N. Over almost all of Europe the magnitude of evaporation is 2-4 mm/day and accounts for 114% of the precipitation signal from 0°E-20°E, 40°N-52°N.

The convergence signal (Fig. 8c) over West Africa is mainly made up of meridional moisture convergence, with zonal convergence dominating on the West African coast at 15°W and 9°N and again in the West African Sahel at 10°W and 12°N. The moisture convergence over West Africa is the main contributor towards precipitation and accounts for ~98% of the precipitation from 15°W-10°E and 5°N -15°N. Over Europe the convergence signal forms a dipole, with positive moisture convergence along the northern coast of the Mediterranean and south of the Alps. This dipole is opposite in sign and magnitude to the moisture advection term (Fig. 8d) over Europe, and similarly to

MJ, the convergence and advection terms over Europe cancel each other out so the divergence of the moisture flux over Europe has a negligible contribution to precipitation over Europe. Over West Africa the moisture advection term (Fig. 8d) is almost zero, but zonal moisture advection does account for ~3% of the precipitation signal from 15°W-10°E and 5°N -15°N.

The transient eddy term (Fig. 8e) over West Africa is small, and negative between 5°N and 12°N, but slightly positive over the Sahara (up to 6 mm/day) due to meridional transient eddies, but the positive transient eddies are negated by negative meridional moisture advection in over the Sahara due to the dry air over the Saharan dessert. The residual term (Fig. 8f), which is accounts for both orographic precipitation and numerical error is small over West Africa, with positive residual contributions towards precipitation over the Cameroon highlands at 10°E, 5°N. Over Europe the transient eddies are positive on the windward side of the Alps between 0°E and 15°E and 42°N to 47°N, and also over the secondary European precipitation maxima at 5°E, between 57°N and 62°N. The residual term (Fig. 8f) resembles the pattern of topography over Europe (similarly to MJ), most likely due to orographic precipitation.

Figure 9a shows the JAS precipitation anomaly. Precipitation is decreased by 3-5 mm/day from 8°N to 15°N across West Africa from 15°W to 20°E. This is equivalent to a reduction in rainfall of 30-50%. Over Europe the maximum precipitation reduction is 3-4 mm/day over the Alps at about 42°N from 5°E to 11°E. European decreases in rainfall correspond to 70-80% from 10°W-20°E and 37°-42°N and 30-60% from 0°E-20°E and 42°-65°N. The evaporation anomaly (Fig. 9b) is negligible over West Africa, but over Europe decreases in precipitation of up to 1 mm/day represent 78% of the precipitation

anomaly from 10°W-20°E and 40°N-55°N. There are also decreases in evaporation over the Mediterranean, even though no SSTA was applied there, of up to 3 mm/day.

The moisture convergence anomaly (Fig. 9c) has a dipole signal over West Africa from 10°N to 20°N, with two additional areas of positive convergence on the coasts, one at about 10°W from 5°N to 11°N, and the other over the Cameroon highlands at 10°E and 5°N. The negative moisture convergence anomaly is mainly supported by the zonal component, and we will see in the circulation figures (Fig. 10) that there is decreased westerly flow into the rainband. The positive moisture convergence anomalies at 15°N - 20°N, 20°W-20°E are mainly supported by the meridional component, and are over compensated for by negative anomalies in the meridional component of moisture advection (Fig, 9d), but the positive moisture convergence anomalies at 5°N-11°N, 10°W and 5°N, 10°E are supported by the zonal component, and they are compensated for by anomalies in the zonal component of the moisture advection.

Over Europe the moisture convergence anomaly (Fig. 9c) has a similar dipole pattern of drying on the windward side of topography and wetting on the leeward side as MJ (Fig. 6c), but the magnitude of the signal in JAS is one half the magnitude of the signal in MJ. Furthermore, in JAS the dipole signal is mainly supported by the zonal component, whereas in MJ it was supported by the meridional component. There is also a moisture convergence dipole anomaly over the Scandanavian countries, at 8°E, between 57°N and 62°N. The meridional component of this anomaly supports the drying and the zonal component supports the wetting, and this signal is compensated for, in sign and magnitude, by the moisture advection anomaly (Fig. 9d).

30

The transient eddy anomalies (Fig. 9e) over West Africa are small except for a band of positive contributions towards rainfall around 19°N across the whole analysis domain. These anomalies of 1-2 mm/day are made up of smaller anomalies in both the zonal and meridional component and are compensated by negative anomalies in the evaporation (Fig. 9b), meridional moisture advection (Fig. 9d) and the residual term (Fig. 9f). The residual anomaly itself is small over all of West Africa, with the biggest anomalies of 2-4 mm/day drying over the Cameroon highlands (5°N, 10°E) and the Guinean highlands (6°N-10°N, 10°W). The transient eddy anomalies over Europe are also small; with some increases in contribution towards precipitation over the Mediterranean due to the meridional component, and some drying on the leeward side of the Alps, also due to the meridional component.

Circulation

Figure 10a shows the future simulation JAS 850 hPa geopotential heights (gpm) and winds (m/s) for the future shutdown and Figure 10b shows the anomalous 850 hPa wind (m/s) and normalized anomalous geopotential height field (gpm), calculated in the same manner as MJ. The future simulated NASH is centered in the same location as the control simulation NASH, however it is intensified over the whole domain, and stretched towards the northeast so that it extends further over Europe than the control simulation, and the heat low over central Africa centered at about 10°N, 20°E, does not extend as far west. As we can see in the anomaly field (Fig. 10b), in which the geopotential height anomaly has been normalized to exclude the overall increase in geopotential heights compared to the control simulation, the intensification and northeast extension of the

NASH creates an anomalous anticyclone with a northeast tilted axis across the northern part of the domain, with the greatest increases in geopotential height over northern Europe and at the western edge of the domain, while the heat low is weakened. This anomalous anticyclone increases westerly flow across the whole domain north of 50°N. The intensified westerly flow is consistent with the increased orographic precipitation and moisture advection on the windward side of European topography that was shown in Fig. 9. The increased westerly flow also has a stronger geostrophic component than the control simulation, which is evident by the decrease in zonal moisture convergence (Fig. 9c) over Europe.

At 600 hPa (Fig. 10c) the Saharan high is intensified in the shutdown compared to the control, just as in MJ. And, as in MJ, the ridge of high pressure over the ocean, associated with an increased NASH throughout the depth of the atmosphere is slightly weaker compared to the overall increases to the Saharan high, as we see in Figure 10d, the 600 hPa normalized anomaly field. In the 600 hPa JAS anomaly the geopotential height increase is greatest over northern Europe and at the western edge of the domain, and there are geopotential height decreases over the North Atlantic and Northern Africa. Similarly to MJ the NASH is intensified, while the Saharan high is weakened. However, unlike MJ, the anomaly patterns at 850 hPa (Fig. 10b) and at 600 hPa (Fig. 10d) show that there may also be a westward intensification of the NASH outside of the analysis domain.

The anomalous anticyclonic flow in the future simulation enhances the northerly winds coming from Europe across the Mediterranean and into West Africa, which because of the decreases in evaporation (Fig. 9b) is consistent with the meridional

32

moisture advection anomalies (Fig. 9d) contributing to drying across West Africa. The anomalous anticyclone also produces anomalous easterly flow across the West African Sahel, west of 20°E, and anomalous northerly flow west of 10°E and south of 5°N which decreases the westerly and southerly flow coming into West Africa to support the monsoon rainfall.

Chapter 6: Conclusions

For this study, examining the effects of global warming and a shutdown of the AMOC, the WRF model was run at 90km horizontal resolution under present-day conditions and forced by late-century A2 CO_2 conditions with an SST anomaly based on the results of water-hosing experiments (e.g.Stouffer et al. 2006, Velling and Wood 2002, 2008) in order to study the climate effects of global warming and an AMOC shutdown on West African and European climate. A caveat to this study is that the AMOC shutdown and global warming forcings are both acting in concert with one another. Separating the two forcings has been done in the literature, but not on a regional or seasonal scale. Future work should also investigate the importance of warming in the South Atlantic and its contribution to the precipitation response in the case of an AMOC shutdown

Reductions in rainfall of up to 80% over southern Europe (Spain and Italy) and 20-40% over northern Europe are associated with an eastward extension of the North Atlantic subtropical high. Over West Africa, reductions in rainfall of 20-40% occurred over the Guinean coast the 70% in the Sahel in the spring; and 30%-50% reductions in precipitation in the Sahel in the summer and are also associated with the changes in the intensity and location of the NASH.

In both the spring and summer the changes in rainfall are consistent with the intensification of geopotential heights and extension of the North Atlantic subtropical high north and eastward over Europe, reminiscent of the wintertime NASH mode, where the high is relatively stronger over the land than the ocean due to the relative changes in cooling over land versus ocean. Both seasons also show a weakened heat low over West

Africa and a weakened Saharan high. The shape and intensity of the anomaly differ between the seasons, but over West Africa both seasonal anomalies are consistent with reduced zonal moisture convergence and meridional moisture advection to support West African rainfall. Over Europe the anomalous anticyclonic flow reduces meridional moisture convergence in the spring and zonal moisture convergence in the summer. The changes in North Atlantic SST lead to decreased evaporation over Europe and the North Atlantic in both seasons, which is consistent with decreased moisture advection and transient eddy rainfall.
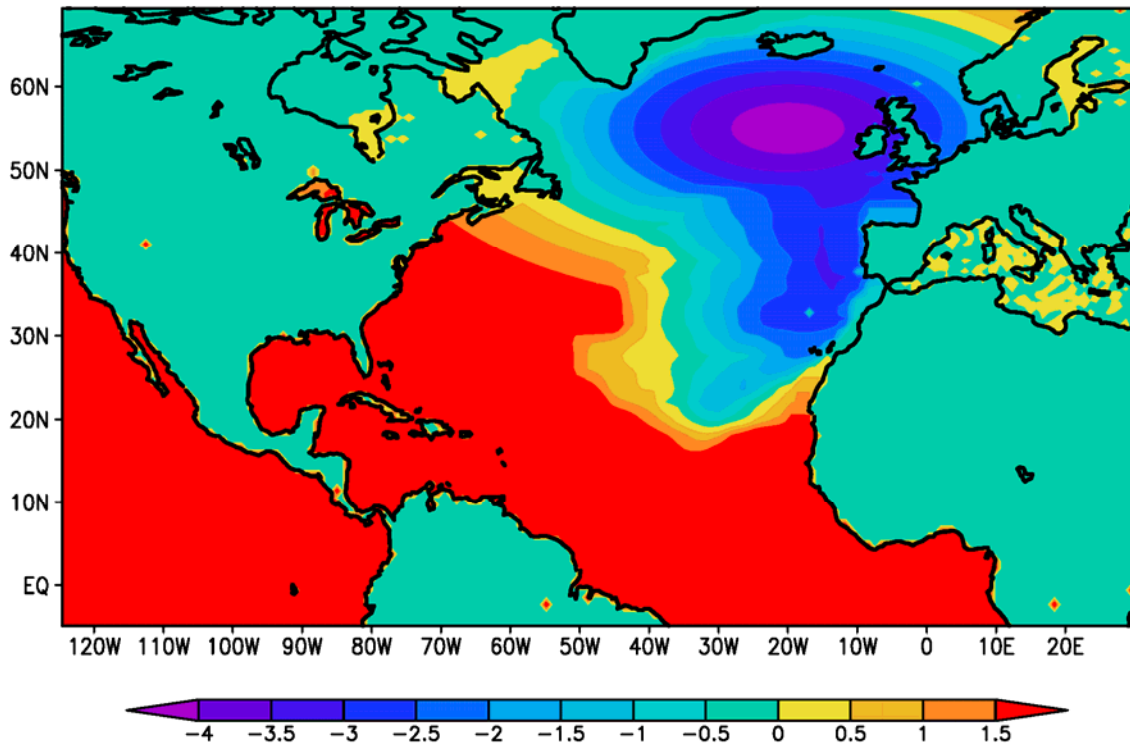
Figure1. The full model domain and sea-surface temperature anomaly (K).
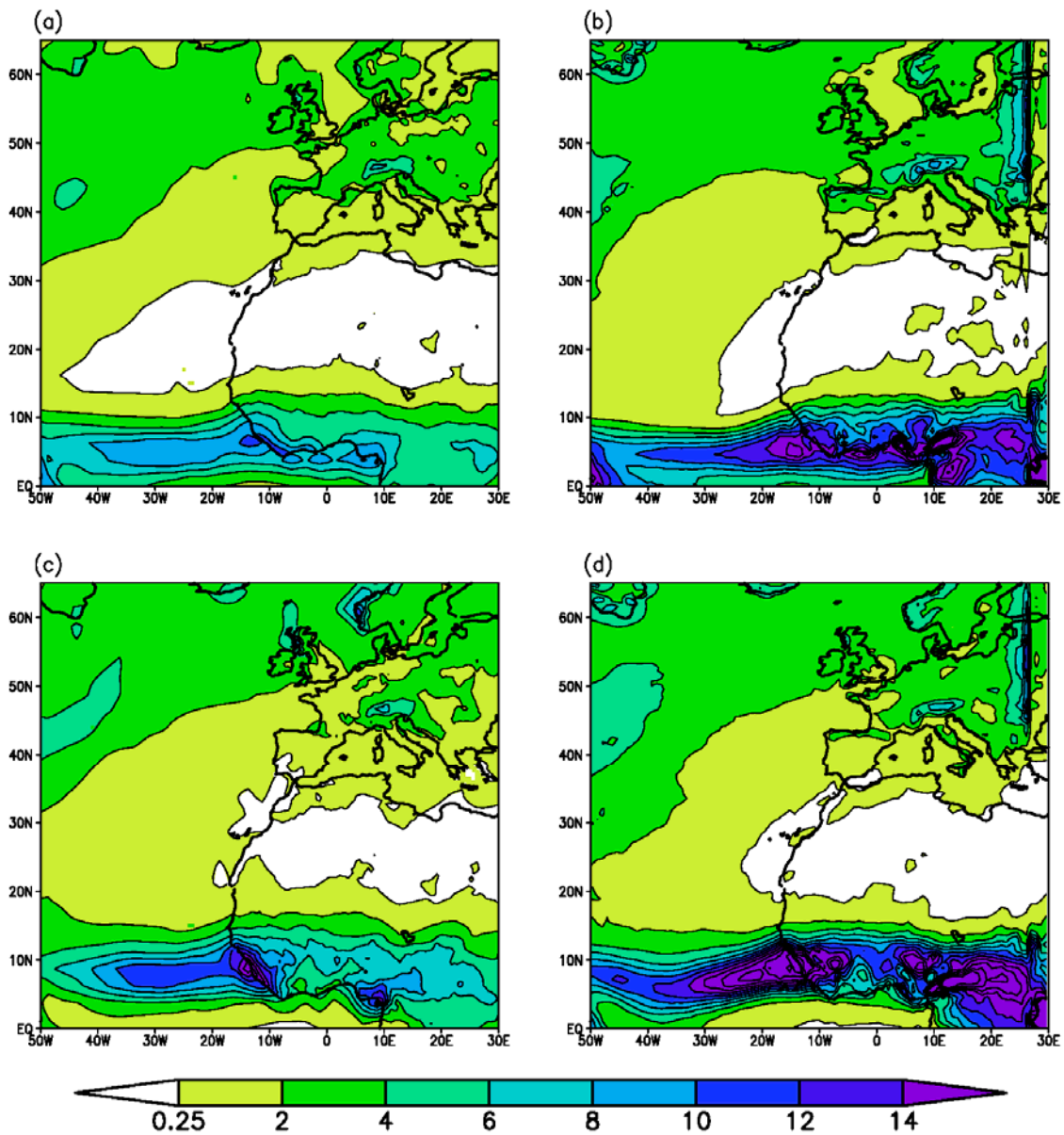
Figure 2. May/June precipitation (mm day^{-1}) from the (a) 1981-2000 CRU climatology over land and the 1981-2000 NASA GPCP V2.1 climatology over water, and (b) 20th century control climatology. Also July – September precipitation for the (c) 1981-2000 CRU/GPCP climatology and (d) 20th century control climatology. Contour interval is 2 mm/day in all panels.
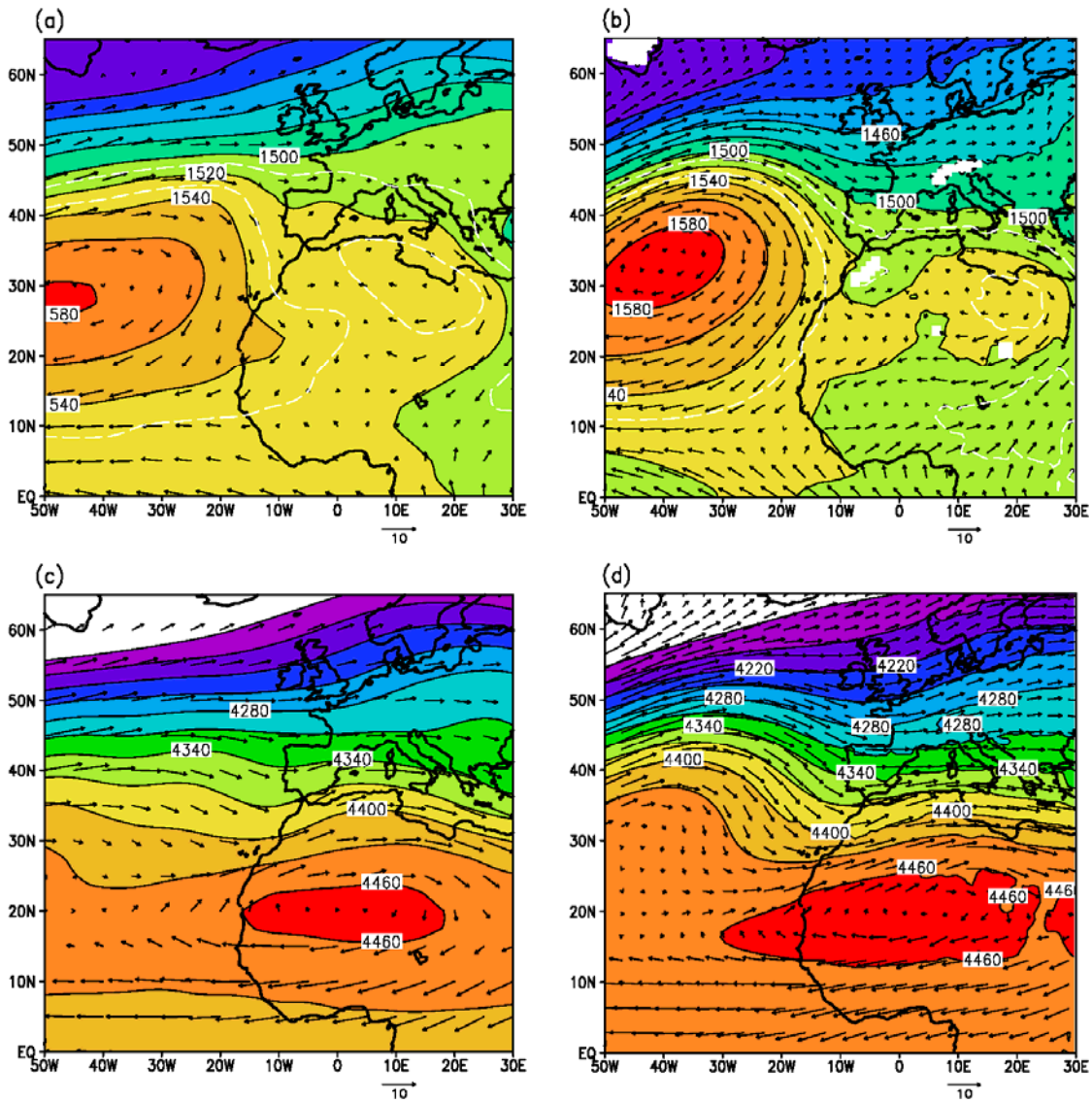
Figure 3. May/June 850 hPa geopotential height (gpm) and winds (m s^{-1}) from the (a) 1979-2009 NCEP2 renalysis climatology, contoured every 20 gpm, with 1510 gpm and 1530 gpm in dashed lines, and (b) 20th century control climatology, also contoured every 20 gpm, with 1510 gpm and 1530 gpm dashed in. May/June 600 hPa geopotential height and winds from the (c) 1979-2009 NCEP2 renalysis climatology countoured at every 30 gpm, and (d) 20th century control climatology, also contoured at every 30 gpm.
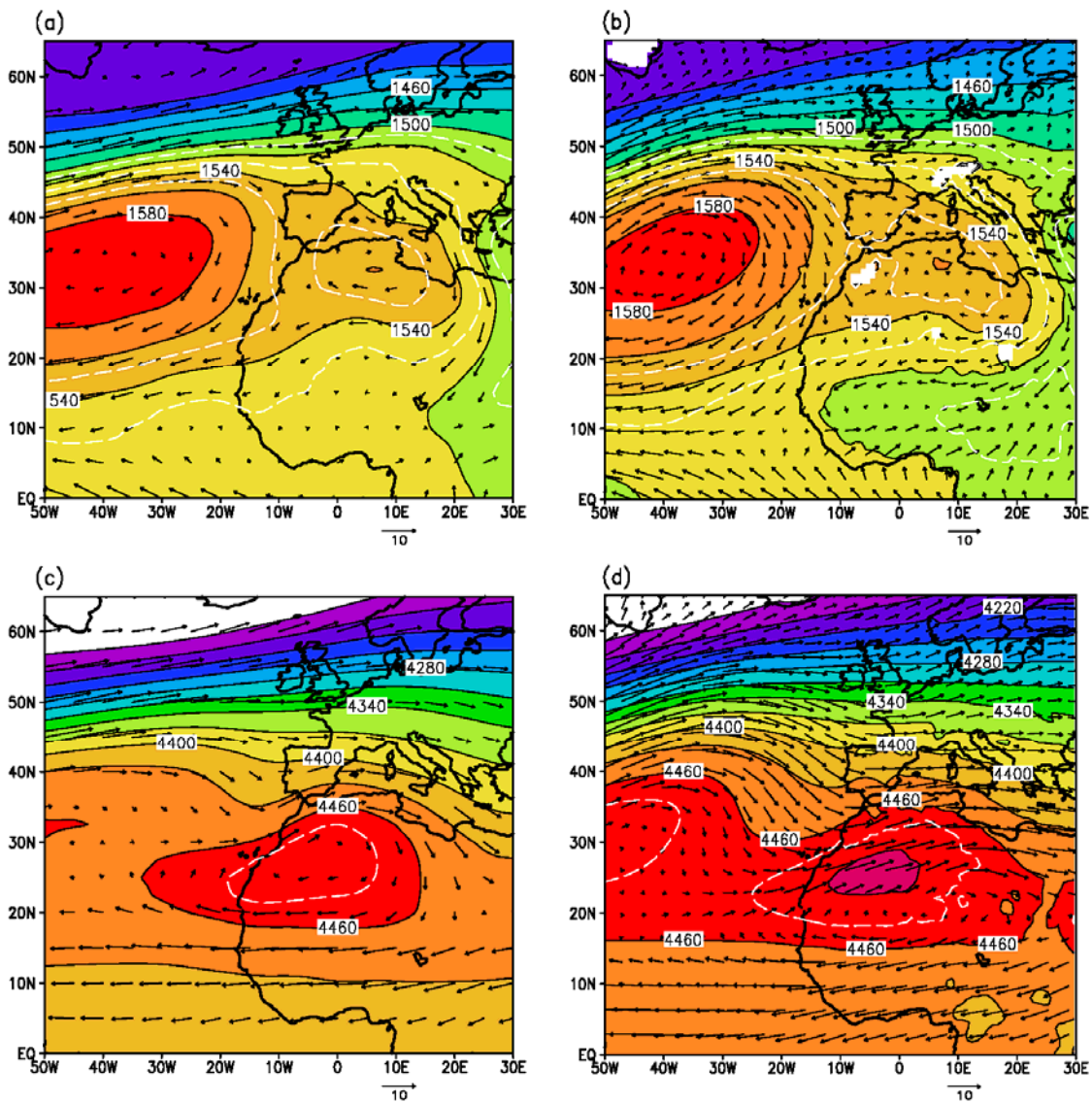
Figure 4. July-September 850 hPa geopotential height (gpm) and winds (m s^{-1}) from the (a) 1979-2009 NCEP2 reanalysis climatology contoured every 20 gpm, with 1510, 1530 and 1550 gpm in dashed lines, and (b) 20th century control climatology, also contoured at 20 gpm intervals with 1510, 1530 and 1550 gpm dashed in. July-September 600 hPa geopotential height and winds from the (c) 1979-2009 NCEP2 renalysis climatology contoured every 30 gpm with 4475 gpm dashed in, and (d) 20th century control climatology, also contoured at a 30 gpm interval with 4475 gpm shown in the dashed line.
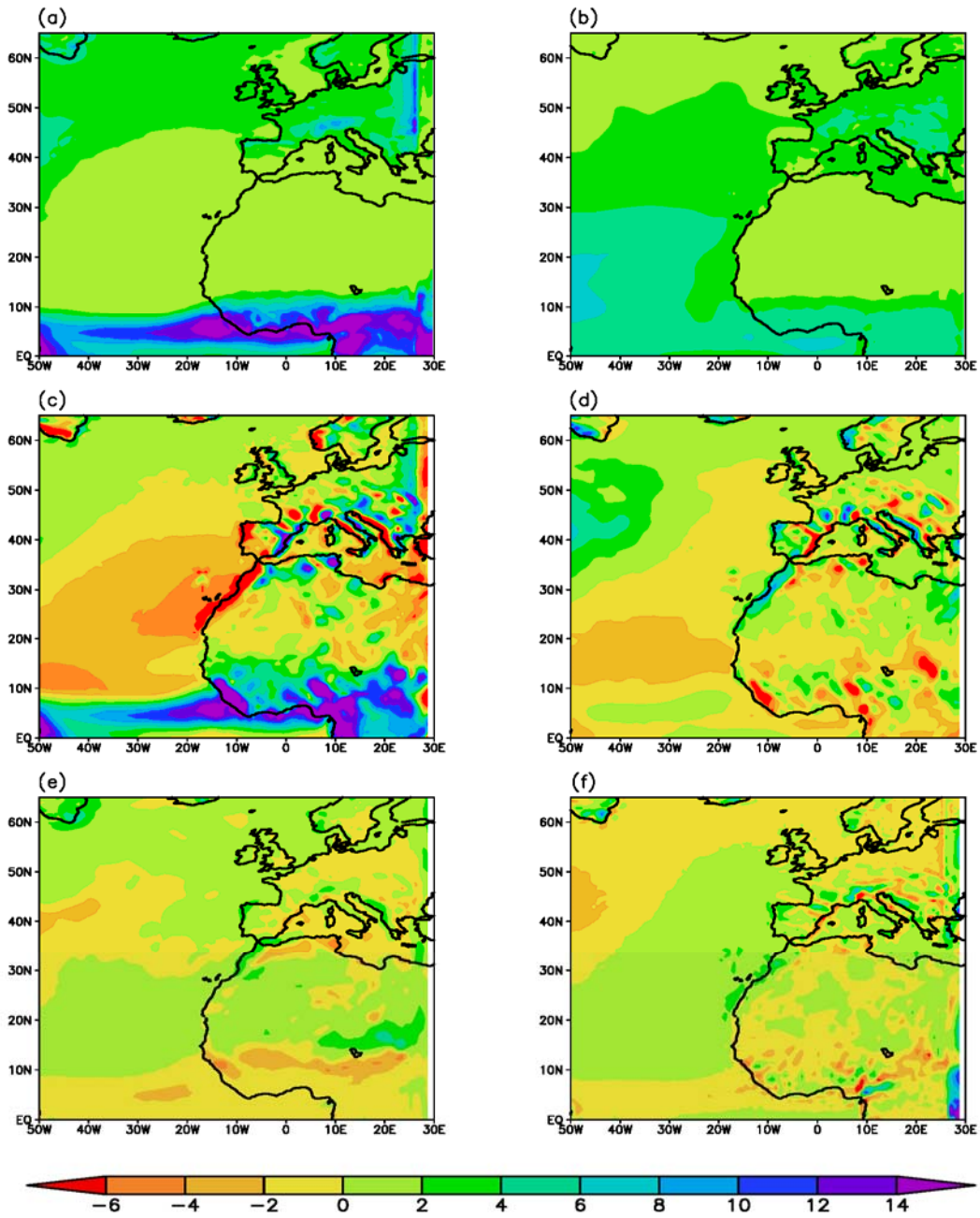
Figure 5. MJ control simulation vertically-integrated, mass-weighted moisture budget (mm/day) (a) precipitation, (b) evaporation, (c) convergence, (d) advection, (e) transient eddies, and (f) orographic residual terms. Each panel is shaded at an interval of 2 mm/day to show that term's contribution towards preciptation.
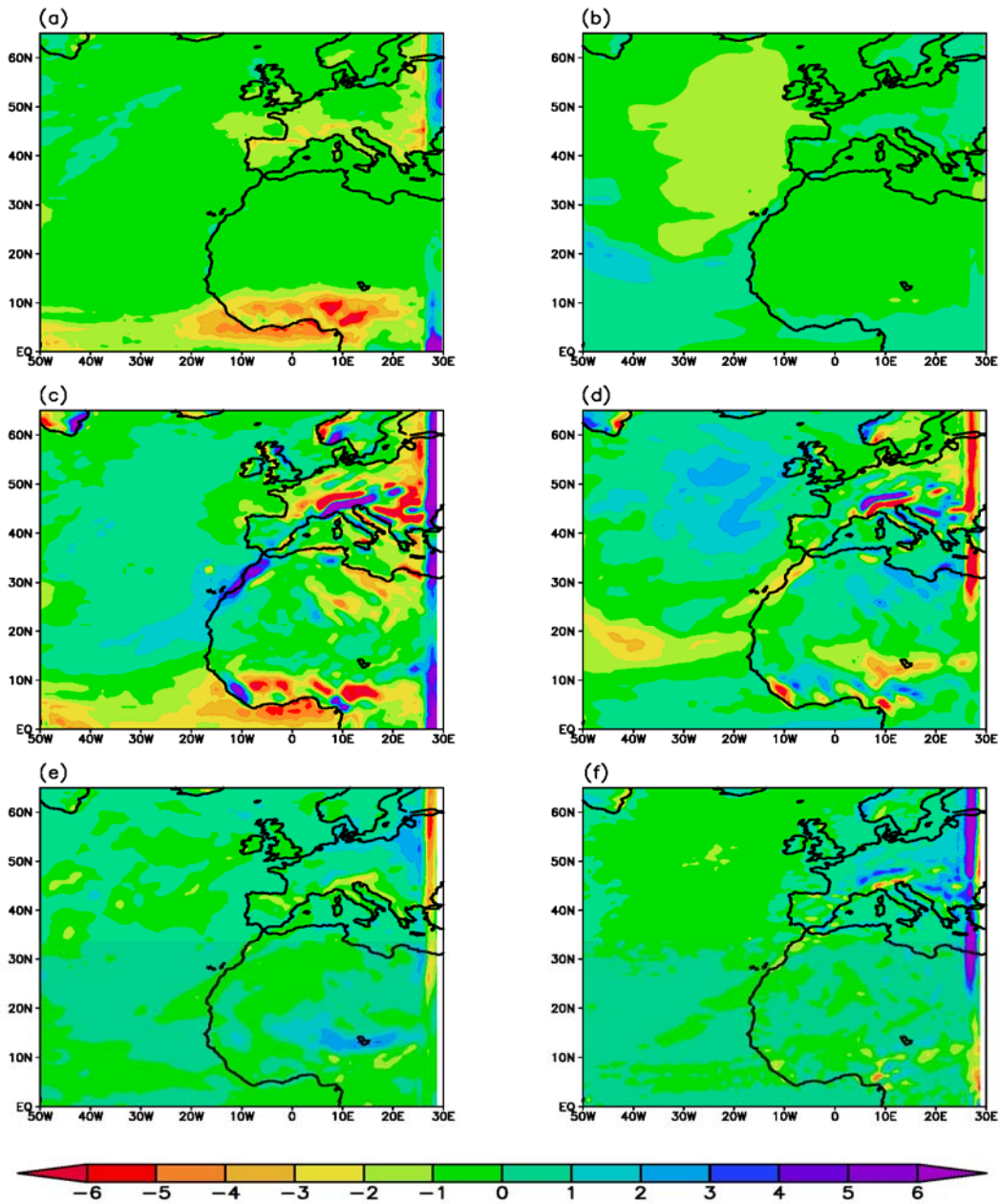
Figure 6. MJ vertically-integrated, mass-weighted moisture budget for the future AMOC shutdown minus 20th century control anomaly (mm/day) for the (a) precipitation, (b) evaporation, (c) convergence, (d) advection, (e) transient eddies, and (f) orographic/residual term. As in Figure 4, each panel is shaded every 1 mm/day to show that term's contribution towards precipitation.
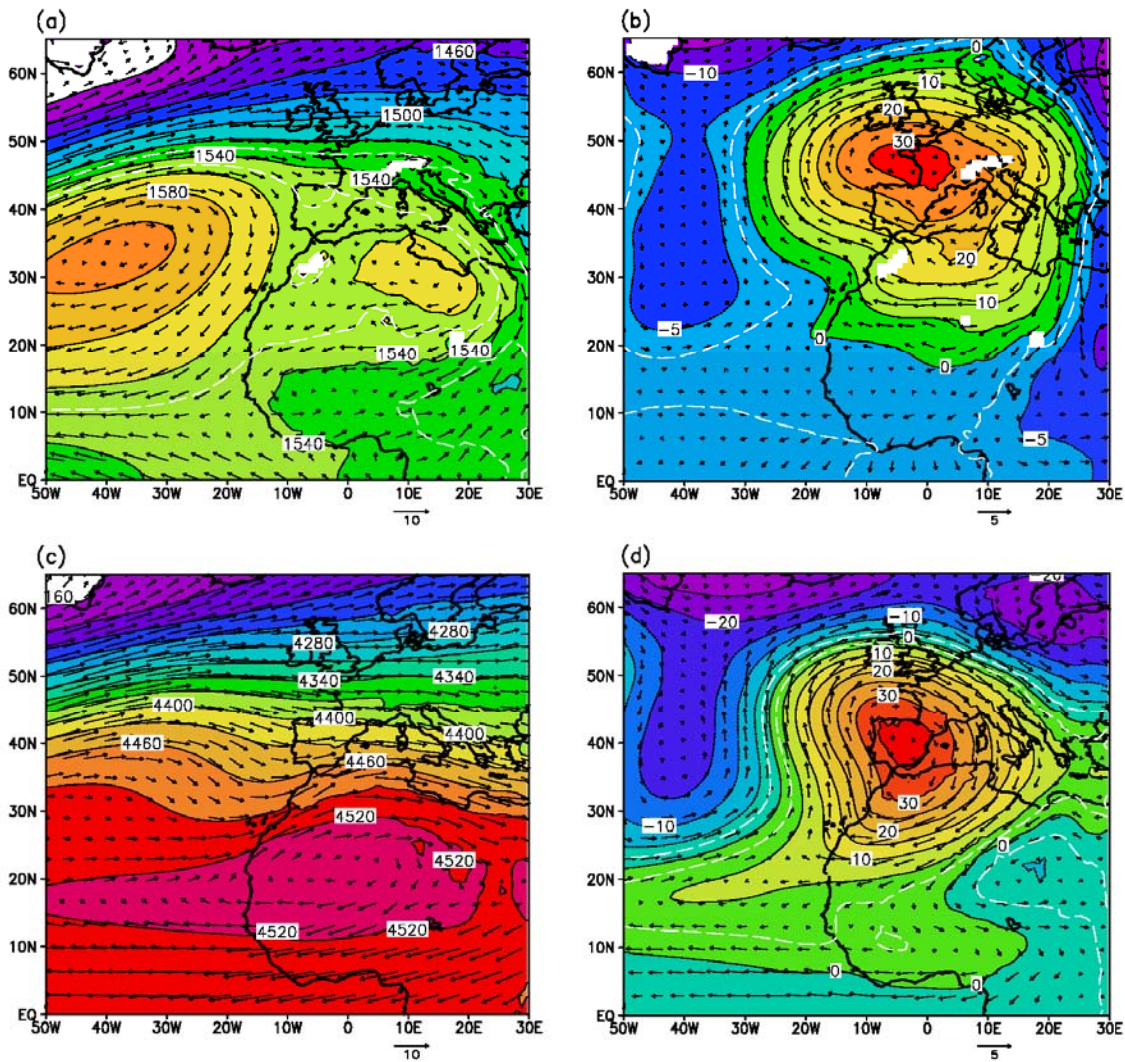
Figure 7. May-June 850 hPa geopotential heights (gpm) and winds (m s^{-1}), (a) future AMOC shutdown simulation climatology contoured every 20 gpm with dashed lines at 1530 and 1550 gpm, and (b) future AMOC shutdown minus 20th century control anomalous winds and normalized anomalous geopotential heights, contoured every 5 gpm, with -2.5 gpm dashed in. May-June 600 hPa geopotential heights (gpm) and winds (m s^{-1}), (c) future AMOC shutdown simulation climatology, contoured at every 30 gpm, and (d) future AMOC shutdown minus 20th century control anomalous winds and normalized anomalous geopotential heights, contoured every 5 gpm, with -2.5 and 2.5 gpm dashed in.
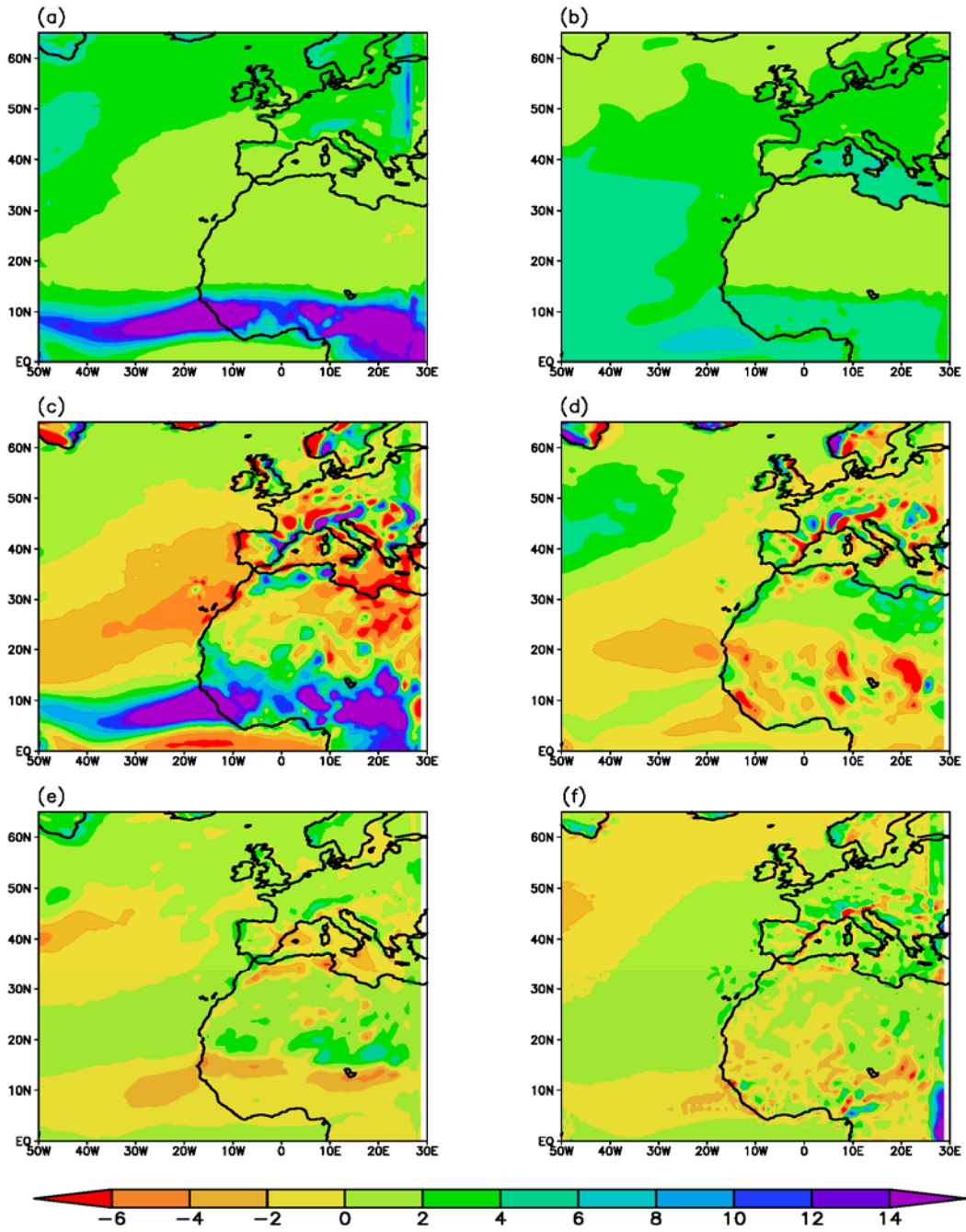
Figure 8. JAS control simulation vertically-integrated, mass-weighted moisture budget (mm/day) (a) precipitation, (b) evaporation, (c) convergence, (d) advection, (e) transient eddies, (f) residual term. Same shading as Figure 5.
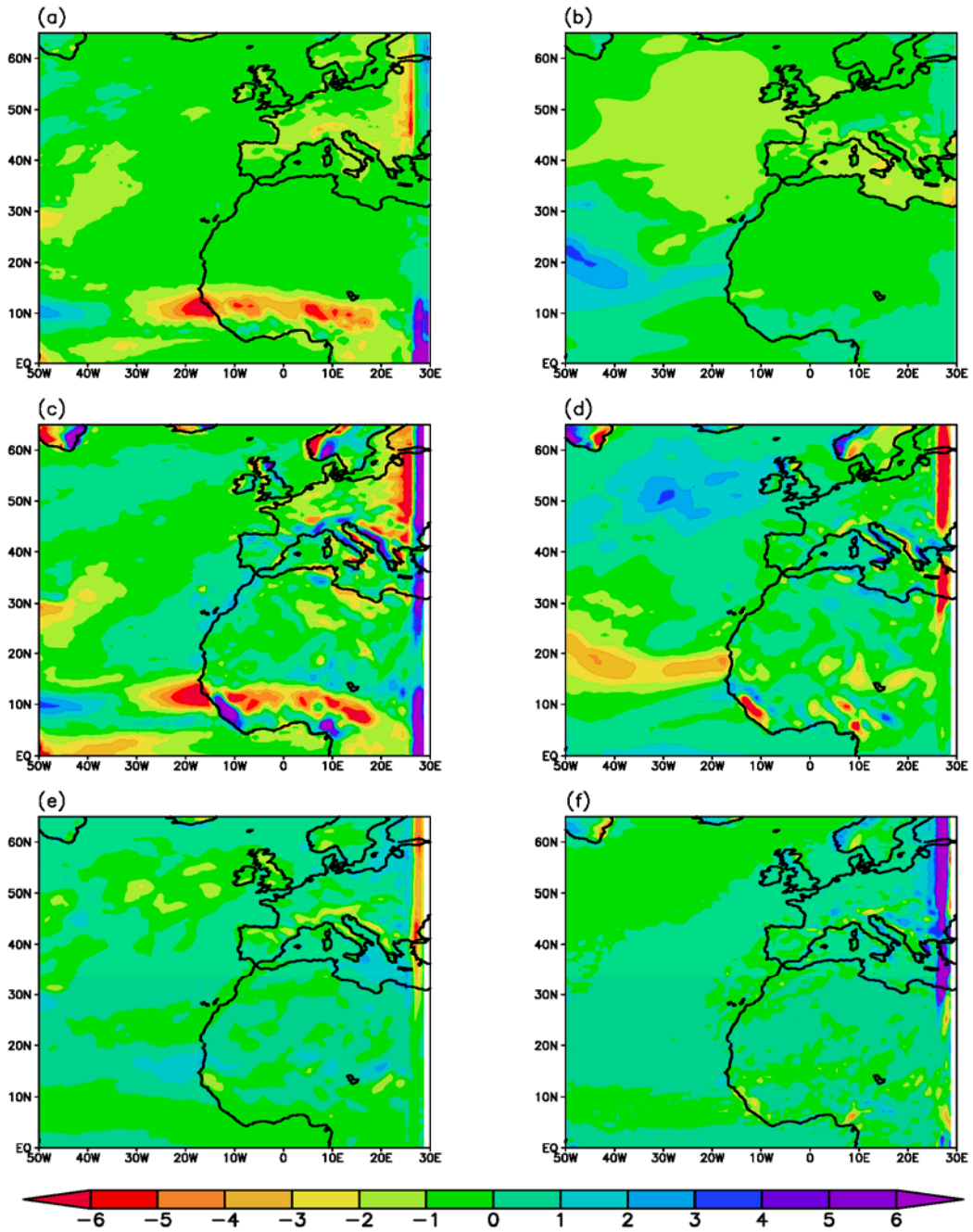
Figure 9. JAS vertically-integrated, mass-weighted moisture budget anomaly (mm/day)
(a) precipitation, (b) evaporation, (c) convergence, (d) advection, (e) transient eddies, (f)
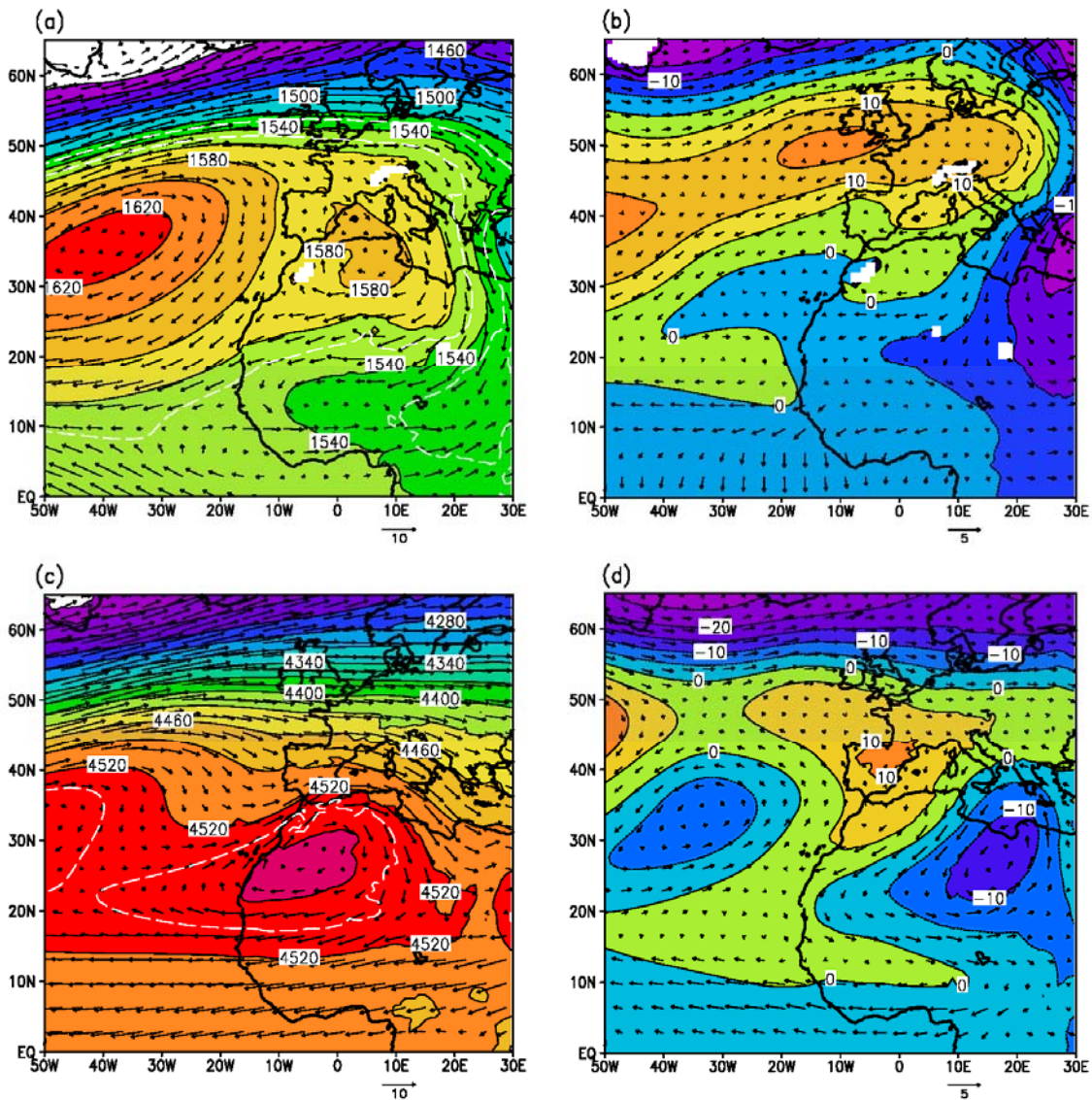residual term. Same shading Figure 6.

Figure 10. July -September 850 hPa geopotential heights (gpm) and winds (m s^{-1}), (a) future shutdown simulation climatology contoured every 20 gpm with dashed lines at 1530 and 1550 gpm, and (b) anomalous wind climatology and normalized anomalous geopotential heights climatology, contoured every 5 gpm. July -September 600 hPa geopotential heights (gpm) and winds (m s^{-1}), (c) future shutdown simulation climatology, contoured every 30 gpm with 4535 gpm dashed in, and (d) anomalous wind climatology and normalized anomalous geopotential heights climatology contoured every 5 gpm.

References

Adler, R.F., G.J. Huffman, A. Chang, R. Ferraro, P. Xie, J. Janowiak, B. Rudolf, U. Schneider, S. Curtis, D. Bolvin, A. Gruber, J. Susskind, P. Arkin, 2003: The Version 2 Global Precipitation Climatology Project (GPCP) Monthly Precipitation Analysis (1979-Present). *J. Hydrometeor.*, **4**, 1147-1167

Barreiro, M., A. Fedorov, R. Pacanowski, and S. G. Philander, 2008: Abrupt climate changes: How freshening of the northern Atlantic affects the thermohaline and wind-driven oceanic circulations. *Annu. Rev. Earth Planet. Sci.*, **36**, 33-58.

Brayshaw, D. J., T. Woollings, and M. Vellinga, 2009: Tropical and Extratropical Responses of the North Atlantic Atmospheric Circulation to a Sustained Weakening of the MOC. *J. Clim.*, **22**, 3146-3155

Chang, P., R. Zhang, W. Hazeleger, C. Wen, X. Wan, L. Ji, R. J. Haarsma, W.-P. Breugem, and H. Seidel, 2008: Oceanic link between abrupt changes in the North Atlantic Ocean and the African monsoon. *Nature Geoscience*, **1**, 444-448.

Chen, F. and J. Dudhia, 2001: Coupling an advanced land-surface/hydrology model with the Penn State/NCAR MM5 modeling system. Part I: model description and implementation. *Mon. Weather Rev.*, **129**, 569-585.

Chen, S.H. and W.Y. Sun, 2002: A one-dimensional time dependent cloud model. *J. Meteorol. Soc. Jpn.*, **80**, 99-108

Clark, P. U., N. G. Pisias, T. F. Stocker, and A. J. Weaver, 2002: The role of the thermohaline circulation in abrupt climate change. *Nature*, **415**, 863-869

Cook, K. H. and E. K. Vizy, 2006: Coupled model simulations of the West African monsoon system: 20th century simulations and 21st century predictions. *J. Clim.*, **19**, 3681-3703

Cook, K. H. and E. K. Vizy, 2008: Effects of twenty-first-century climate change on the Amazon rain forest. *J. Clim.*, **21**, 542-560

Davis, R. E., B. P. Hayden, D. A. Gay, W. L. Phillips, and G. V. Jones, 1997: The North Atlantic subtropical anticyclone. *J. Clim.*, **10**, 728-744

Drijfhout, S. S., 2010: The Atmospheric Response to a Thermohaline Circulation Collapse: Scaling Relations for the Hadley Circulation and the Response in a Coupled Climate Model. *J. Clim.*, **23**, 757-774

Dudhia, J., 1989: Numerical study of convection observed during the winter monsoon experiment using a mesoscale two-dimensional model. *J. Atmos. Sci.*, **46**, 3077-3107

Fichefet, T., C. Poncin, H. Goosse, P. Huycrechts, I. Janssens, and H. Le Treut, 2003: Implications of changes in freshwater flux from the Greenland ice sheet for the climate of the 21st century. *Geophys. Res. Lett.*, **30**, 1911-1914

Folland, C. K., T. N. Palmer, and D. E. Parker 1986: Sahel rainfall and worldwide sea temperatures. 1901-85 *Nature*, **320**, 602-607

Ganopolski, A., S. Rahmstorf, V. Petoukhov, and M. Claussen, 1998: Simulation of moden and glacial climates with a coupled global model of intermediate complexity. *Nature*, **391**, 351-356

Gerdes, R. W. Hurlin, and S. M. Griffies, 2006: Sensitivity of a global ocean model to increased run-off from Greenland. *Ocean Model*, **12**, 416-435

Hu, A., G. A. Meehl, W. M. Washington, and A. Dai, 2004: Response of the Atlantic thermohaline circulation to increased atmospheric CO_2 in a coupled model. *J. Clim.*, **17**, 4267-4279

Hu, A., G. A. Meehl, W. Han, and J. Yin, 2011: Effect of the potential melting of the Greenland Ice Sheet on the Meridional Overturning Circulation and global climate in the future. *Deep-Sea Research.*, **58**, 1914-1926

Jacob, D., H. Goettel, J. Jungclaus, M. Muskulus, R. Podzun, and J. Marotzke, 2005: Slowdown of the thermohaline circulation causes enhanced maritime climate influence and snow cover over Europe. Geophys. Res. Lett., 32, L21711

Janjic, Z.I., 1990: The step-mountain coordinate: physical package. *Mon. Weather Rev.*, **118**, 1429-1443

Janjic, Z.I., 1994: The step-mountain Eta coordinate model: further developments of the convection, viscous sublayer and turbulence closure schemes. *Mon. Weather Rev.*, **122**, 927-945

Janjic, Z.I., 1996: The surface layer in the NCEP Eta Model. In: Eleventh conference on numerical weather prediction. Norfolk, VA, 19-23 August 1996. Amer. Meteor. Soc., Boston, MA, pp 354-355

Janjic, Z.I., 2002: Nonsingular implementation of the Mellor-Yamada Level 2.5 Scheme in the NCEP Meso model. *NCEP Office Note No. 437*, 61 pp

Junclaus,J. H., H. Haak, M. Esch, E. Roeckner, and J. Marotzke, 2006: Will Greenland melting halt the thermohaline circulation. *Geophys. Res. Lett.*, **33**, L17708

Kain, J.S. and J.M. Fritsch, 1990: A one-dimensional entraining detraining plume model and its application in convective parameterization. *J. Atmos. Sci.*, **47(23)**, 2784-2802

Kain, J.S. and J.M. Fritsch, 1993: Convection parameterization for mesoscale models: the Kain-Fritsch scheme. The representation of cumulus convection in numerical models. *Meteor. Monogr.*, **24**, 165-170

Kanamitsu, M., W. Ebisuzaki, J. Woollen, S. K. Yang, J. J. Hnilo, M. Fiorino and G. L. Potter, 2002: NCEP-DOE AMIP-II reanalysis (R-2). *Bull. Amer. Meteorol. Soc.*, **83**, 1631-1643

Kulhbrodt, T., S. Rahmstorf, K. Zickfeld, F. B. Vikebø, S. Sundby, M. Hoffman, P. M. Link, A. Bondeau, W. Cramer, and C, Jaeger, 2009: An integrated assessment of changes in the thermohaline circulation, *Clim. Change*, **96**, 489-537

Lamb, P. J., 1978: Case studies of Tropical Atlantic surface circulation patterns during recent sub-Saharan weather anomalies: 1967 and 1968. *Mon. Weather Rev.*, **106**, 482-491

Latif, M., E. Roeckner, U. Mikolajewicz, and R. Voss, 2000: Tropical Stabilization of the Thermohaline Circulation in a Greenhouse Warming Simulation. *J. Clim.*, **13**, 1809-1813

Laurian, A., S. S. Drijfhout, and W. Hazeleger, 2009a: Response of the Western European climate to a collapse of the thermohaline circulation. *Clim. Dynam.*, **43**, 689-697

Laurian, A. S. S. Drijfhout, W. Hazeleger, and R. van Dorland, 2009b: Global surface cooling: The atmospheric fast feedback response to a collapse of the thermohaline circulation. *Geophys. Res. Lett.*, **36**, L20708

Laurian, A. and S. S. Drijfhout, 2011: Response of the South Atlantic circulation to an abrupt collapse of the Atlantic meridional overturning circulation. *Clim. Dynam.*, **37**, 521-530

Lenters, J. D. and K. H. Cook, 1995: Simulation and diagnosis of the regional summertime precipitation climatology of South America. *J. Clim.*, **8**, 2988-3005

Lenton, T. M., H. Held, E. Kriegler, J. W. Hall, W/ Lucht, S. Rahmstorf, and H. J. Schellenhuber, 2008: Tipping elements in the Earth's climate system. *Proc. Natl. Acad. Sci. USA*, **105**, 1786-1793

Lin, Y. L., R. D. Farley, and H. D. Orville, 1983: Bulk parameterization of the snow field in a cloud model. *J. Appl. Meteorol.*, **22**, 1065-1092

Manabe, S. and R. J. Stouffer, 1988: Two stable equilibria of a coupled ocean atmosphere model. *J. Clim.*, **1**, 841-866

Manabe, S. and R. J. Stouffer, 1994: Multiple century response of a coupled ocean-atmosphere model to an increase of atmospheric carbon dioxide. *J. Clim.*, **7**, 5-23

Manabe, S. and R. J. Stouffer, 1995: Simulation of abrupt climate change induced by freshwater input to the North Atlantic Ocean. *Lett. to Nat.*, **378**, 165-167

Meehl, G. A., T. F. Stocker, W. D. Collins, P. Friedlingstein, A.T. Gaye, J. M. Gregory, A. Kitoh, R. Knutti, J. M. Murphy, A. Noda, S. C. B. Raper, I. G. Watterson, A. J. Weaver, and Z-C Zhao, 2007: Global climate projections In: Solomon, S., D. Qin, M. Manning, Z. Chen, M. Marquis, K. Averyt, M. Tignor, Miller (eds) Climate change 2007: the physical science basis. Contribution of working group I to the fourth assessment report of the intergovernmental panel on climate change. Cambridge University Press, Cambridge, MA

Mellor, G. L. and T. Yamada, 1982: Development of a turbulence closure model for geophysical fluid problems. *Rev. Geophys.*, **20**, 851-875

Mitchell, T. D., and P. D. Jones, 2005: An improved method of constructing a database of monthly climate observations and associated high-resolution grids. *Int. J. Climatol.*, **25**, 693-712

Mlawer, E. J., S. J. Taubman, P. D. Brown, M. J. Iacono, and S. A. Clough, 1997: Radiative transfer for inhomogeneous atmosphere: RRTM, a validated correlated-k model for the longwave. *J. Geophys. Res.*, **102(D14)**, 16663-16682

Monin, A. S, and A. M. Obukhov, 1954: Basic laws of turbulent mixing in the surface layer of the atmosphere. *Contrib. Geophys. Inst. Acad. Sci. USSR*, **151**, 163-187 (in Russian)

Neupane, N. and K. H. Cook, 2011: Nonlinear response of Sahel rainfall to Atlantic warming: Potential for abrupt climate change. *Submitted to Journal of Climate*

Patricola, C. M., and K. H. Cook, 2010: Northern African climate at the end of the twenty-first century: and integrated application of regional and global climate models. *Clim. Dynam.,* **35**, 193-212

Pu, B., E. K. Vizy, and K. H. Cook: Warm season climate response to the Atlantic meridional overturning circulation shutdown and greenhouse gas warming over North America (in preparation)

Ridley, J. K., P. Huybrechts, J. M. Gregory, and J. A. Lowe, 2005: Elimination of the Greenland Ice Sheet in a high CO_2 climate. *J. Clim.*, **18**, 3409-3427

Rojas, M. and A. Seth, 2003: Simulation and sensitivity in a nested modeling study for South America. Part II. GCM boundary forcing. *J. Clim.*, **16**, 2454-2471

Rutledge, S.A. and P.V. Hobbs, 1984: The mesoscale and microscale structure and organization of clouds and precipitation in midlatitude cyclones. XII: a diagnostic modeling study of precipitation development in narrow cold-frontal rainbands. *J. Atmos. Sci.*, **41(20)**, 2949-2972

Schiller, A., U. Mikolajewicz, and R. Voss, 1997: The stability of the North Atlantic thermohaline circulation in a coupled ocean-atmosphere general circulation model. *Clim. Dynam.*, **13**, 325-347

Schmittner, A., M. Latif, and B. Schneider, 2005: Model projections of the North Atlantic thermohaline circulation for the 21st century assessed by observations. *Geophys. Res. Lett.*, **32**, L23710

Seth, A. and M. Rojas, 2003: Simulation and sensitivity in a nested modeling study for South America. Part I. Reanalysis boundary forcing. *J. Clim.*, **16**, 2437-2453

Skamarock, W. C., J. B. Klemp, J. Dudhia, D. O. Gill, D. M. Barker, W. Wang, and J. G. Powers, 2005: A description of the Advanced Research WRF Version 2. *NCAR Tech. Note, ncar/TN-468+STR*, 88 pp

Smirnova, T. G., J. M. Brown, and S. G. Benjamin, 1997: Performance of different soil model configurations in simulating ground surface temperature and surface fluxes. *Mon. Weather Rev.*, **125**, 1870-1884

Smirnova, T. G., J. M. Brown, S. G. Benjamin, and D. Kim, 2000: Parametization of cold season processes in the MAPS land-surface scheme. *J. Geophys. Res.*, **105**, 4077-4086

Stouffer, R. J., J. Yin, J. M. Gregory, K. W. Dixon, A. J. Weaver, M. J. Spelman, W. Hurlin, M. Eby, G. M. Flato, H. Hasumi, A. Hu, J. H. Jungclaus, I. V. Kamenkovich, A. Levermann, M. Montoya, S. Murakami, S, Nawrath, A. Oka, W. R. Peltier, D. Y. Robitaille, A. Sokolov, G. Vettoretti and S. L. Weber, 2006: Investigating the causes of the response of the thermohaline circulation to past and future climate changes. *J. Clim.*, **19**, 1365-1387

Swingedouw, D., P. Braconnot, and O. Marti, 2006: Sensitivity of the Atlantic Meridional Overturning Circulation to the melting from northern glaciers in climate change experiments. *Geophys. Res. Lett.*, **33**, L07711

Swingedouw, D., P. Baconnot, P. Delecluse, E. Guilyardi and O. Marti, 2007: Quantifying the AMOC feedbacks during a 2XCO$_2$ stabilization experiment with land-ice melting. *Clim. Dynam.*, **29**, 521-534

Tao, W. K., J. Simpson, and M. McCumber, 1989: An ice-water saturation adjustment. *Mon. Weather Rev.*, **117**, 231-235

Thorpe, R. B., J. M. Gregory, T. C. Johns, R. A. Wood, and J. F. B. Mitchell, 2001: Mechanisms Determining the Atlantic Thermohaline Circulation Response to Greenhouse Gas Forcing in a Non-Flux-Adjusted Coupled Climate Model. *J. Clim.*, **14**, 3102-3116

Vizcaino, M., U. Mikolajewicz, M. Groeger, E. Maier-Reimer, G. Schurgers and A. M. E. Winguth, 2008: Long-term ice sheet-climate interactions under anthropogenic greenhouse forcing simulated with a complex Earth System Model. *Clim. Dynam.*, **31**, 665-690

Vizy, E.K. and K.H. Cook, 2001: Mechanisms by which Gulf of Guinea and eastern North Atlantic sea surface temperature anomalies can influence African rainfall. *J. Clim.*, **14**, 795-821

Vizy, E. K., and K. H. Cook, 2011: Impact of future climate change on the sub-Saharan Sahel growing season days: A regional climate model perspective. *Submitted to Climate Dynamics*

Vellinga, M. and R.A. Wood, 2008: Impacts of thermohaline circulation shutdown in the twenty-first century. *Clim. Change*, **91**, 43-63

Vellinga, M. and R.A. Wood, 2002: Global climatic impacts of a collapse of the Atlantic thermohaline circulation. *Clim. Change*, **3**, 251-267

Wen, C., P. Chang, and R. Saravanan, 2010: Effect of Atlantic Meridional Overturning Circulation Changes on Tropical Atlantic Sea Surface Temperature Variability: A 2 ½ -Layer Reduced Gravity Ocean Model Study. *J. Clim.*, **23**, 312-332

Wood, R. A., A. B. Keen, J. F. B. Mitchell, and J. M. Gregory, 1999: Changing spatial structure of the thermohaline circulation in response to atmospheric CO_2 forcing in a climate model. *Nature*, **399**, 572-575

Zhang, R., and T. L. Delworth, 2005: Simulated Tropical Response to a Substantial Weakening of the Atlantic Thermohaline Circulation. *J. Clim.*, **18**, 1853-1860